Naval Research Laboratory

Washington, DC 20375-5000

NRL Memorandum Report 6205

Modeling of Ocean Surface Spectrum and Surface Scattering — Applications to Reverberation Prediction in the AAUS Program

T.D.K. NGOC, E.R. FRANCHI AND B.B. ADAMS

Acoustic Systems Branch
Acoustic Division

June 23, 1989

SECURITY CLASSIFICATION OF THIS PAGE

REPORT DOCUMENTATION PAGE

Form Approved
OMB No 0704-0188

1a REPORT SECURITY CLASSIFICATION UNCLASSIFIED	1b RESTRICTIVE MARKINGS
2a SECURITY CLASSIFICATION AUTHORITY	3 DISTRIBUTION AVAILABILITY OF REPORT Approved for public release; distribution unlimited.
2b DECLASSIFICATION / DOWNGRADING SCHEDULE	
4 PERFORMING ORGANIZATION REPORT NUMBER(S) NRL Memorandum Report 6205	5 MONITORING ORGANIZATION REPORT NUMBER(S)
6a NAME OF PERFORMING ORGANIZATION Naval Research Laboratory 6b OFFICE SYMBOL (If applicable) Code 5160	7a NAME OF MONITORING ORGANIZATION
6c ADDRESS (City, State, and ZIP Code) Washington, DC 20375-5000	7b ADDRESS (City, State, and ZIP Code)
8a NAME OF FUNDING / SPONSORING ORGANIZATION Office of Naval Technology 8b OFFICE SYMBOL (If applicable) Code 234	9 PROCUREMENT INSTRUMENT IDENTIFICATION NUMBER
8c ADDRESS (City, State, and ZIP Code) Arlington, VA 22217	10 SOURCE OF FUNDING NUMBERS PROGRAM ELEMENT NO: 62435N PROJECT NO: RJ35B01 TASK NO: RL3A WORK UNIT ACCESSION NO: DN480-045

11 TITLE (Include Security Classification)
Modeling of Ocean Surface Spectrum and Surface Scattering - Applications to Reverberation Prediction in the AAUS Program

12 PERSONAL AUTHOR(S)
Ngoc, T.D.K., Franchi, E.R. and Adams, B.B.

13a TYPE OF REPORT	13b TIME COVERED	14 DATE OF REPORT (Year, Month, Day)	15 PAGE COUNT
	FROM 10/83 TO 9/84	1989 June 23	83

16 SUPPLEMENTARY NOTATION

17 COSATI CODES			18 SUBJECT TERMS (Continue on reverse if necessary and identify by block number)
FIELD	GROUP	SUB-GROUP	(See page ii)

19 ABSTRACT (Continue on reverse if necessary and identify by block number)

Current scattering theories for sound interaction with the ocean surface and empirical descriptions of the ocean surface wave spectrum are examined for incorporation into the NRL Reverberation Model (RASP). The intent is to provide surface scattering strength estimates using such theories to augment the empirical data bases in surface scattering strength already included in RASP. Since the input surface wave spectrum plays a critical role in determining the scattering strength, a comprehensive assessment of available empirical models of surface wave spectra was performed and the most updated version of the Pierson model was selected for use in combination with the azimuthal distribution model proposed by Mitsuyasu et al. The present study was focussed on those scattering theories that perform best in the low frequency (< 500 Hz), low-grazing angle (< 20°) regime. As a result, scattering models such as the small perturbation method and the composite-roughness approach were selected for incorporation into RASP in addition to two empirical models, Martin

(Continues)

20 DISTRIBUTION / AVAILABILITY OF ABSTRACT	21 ABSTRACT SECURITY CLASSIFICATION
☒ UNCLASSIFIED/UNLIMITED ☐ SAME AS RPT ☐ DTIC USERS	UNCLASSIFIED
22a NAME OF RESPONSIBLE INDIVIDUAL L. Bruce Palmer	22b TELEPHONE (Include Area Code) (202) 767-3288 22c OFFICE SYMBOL Code 5160

DD Form 1473, JUN 86 *Previous editions are obsolete* SECURITY CLASSIFICATION OF THIS PAGE

S/N 0102-LF-014-6603

18. SUBJECT TERMS

Reverberation
Sea surface waveheight spectra
Kirchoff approximation
Reverberation models
Surface scattering
Perturbation theory
Composite roughness approximation

19. ABSTRACTS (Continued)

and Chapman-Harris. Illustrations of the surface wave two-dimensional spectrum are presented, and sample computations of the scattering strength using the selected models are given for different combinations of the principal parameters, which include frequency, wind speed, wind direction, and scattering geometry. These newly-developed capabilities satisfy quite adequately immediate computational requirements, and will be incorporated into RASP. Future research needs are also identified which will enable better understanding and prediction of the spectral content and stochastic fluctuations of ocean surface-scattered acoustic fields.

CONTENTS

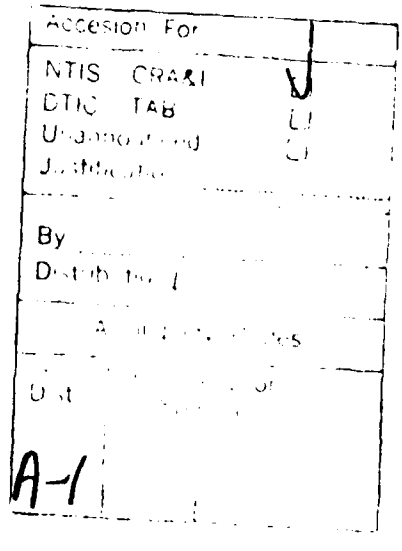

MODELING OF OCEAN SURFACE SPECTRUM AND SURFACE SCATTERING — APPLICATIONS TO REVERBERATION PREDICTION IN THE AAUS PROGRAM

1. Introduction

There are two approaches to modeling long-range reverberation in underwater acoustics: one is to describe reverberation by a multi-element model, of which each element separately treats surface scattering, bottom scattering, propagation within the medium, and complex finite target effects; and the other is to construct a reverberation model essentially as a propagation model in which surface, bottom scattering, and complex target scattering are taken into account via application of appropriate boundary conditions. The modular approach offers a practical flexibility that allows one to take full advantage of a broad range of research advances attained in diversified research areas that are normally investigated independently of each other. For this reason the NRL reverberation model (RASP: Range-dependent Active Systems Prediction Model) is a multi-element model. (For a documentation of RASP, please refer to NRL Report No. 8721, "NRL Reverberation Model: A Computer Program for the Prediction and Analysis of Medium to Long-Range Boundary Reverberation," by E. R. Franchi, J. M. Griffin, and B. J. King, 1984.)

There have been several methods of formulating the surface scattering problem. Some were developed further than others, but each has its own limitations and strengths. In this report, these different methods will be identified either by their solution methodology or by their fundamental assumptions if the same analytical framework is to be taken. The two major methods that have been subject to more extensive investigation are the perturbation and tangent plane methods. In addition to these two, other methods that are built on the concepts of composite-roughness and empirical modeling will be reviewed and assessed in this report. The current effort is thus focused upon those surface scattering models that deal with a randomly rough surface and that are relevant to the modular approach. Therefore, excluded from discussion in this study are research works [J1-J6] treating surface scattering as part of a propagation model (e.g. coupled-mode analysis, transport theory) and those developed for a periodically rough surface.

While RASP is a complete executive routine and model suite capable of handling range dependence, complex surface and bottom geometries, and target characteristics, its operation has been slowed by separate calculations required for surface scattering. To better organize and thereby facilitate the application to extensive data bases and system performance calculations the direct incorporation of several surface scattering submodels has been undertaken. The program has entailed a critical review and assessment of existing models for ocean surface scattering, selection of several surface scattering models that are deemed most suitable and incorporation of these as optional

Manuscript approved April 17, 1989.

submodels addressable by the RASP executive. Selection of the scattering models targeted for detailed examination and earliest incorporation has been guided by the presently prevalent interests in low frequencies, low grazing angles, and long ranges of propagation.

Despite numerous differences among these surface scattering models, predictions made by them are all critically dependent on an adequate understanding of the ocean surface waves. In fact, ocean surface wave spectra as the most important environmental parameter strongly influence the computational results generated by these models. Comparison with experimental measurements and among themselves provide resolution only when ocean surface wave spectra are reasonably understood and specified. Consequently, a comprehensive treatment of the ocean surface wave spectrum is also an essential requirement in making the best use of existing scattering theories as well as in properly including the environmental conditions. Modeling the ocean surface wave spectrum has therefore been considered an integral part of the current program.

Currently, a comprehensive review of surface scattering models has been completed. These scattering theories have been screened and assessed with regard to their relevance to current interests. The scattering models that appear most practically implementable received detailed examination in this report. The existing one- and two-dimensional models of the ocean surface waves have also been reviewed and model subroutines for these surface wave spectra have been established as necessary secondary support for the scattering models. Preliminary application of the developed one- and two-dimensional models for the ocean surface wave spectrum has been implemented for several chosen scattering models.

The general purpose of this report is to document and summarize the research progress made to date on implementing surface scattering acoustic models and their component ocean surface models, as components of RASP. It will also chart out the future research plan for this effort. Section 2 will provide an overview of major methodologies that have been applied to investigate the problem of surface scattering. A detailed examination of the more established scattering models and ocean surface spectrum models adapted for use in the selected scattering models will be presented as appendices to the main text. Section 3 then will assess the relevance of each major scattering model. In Section 4, computational examples of several scattering models combined with the chosen ocean surface descriptions will be illustrated. The final section, Section 5, will summarize the key conclusions and planned future efforts. Also provided is a selected bibliography, in which key references of the same research focus are grouped together at the authors' discretion.

2. Alternative Methodologies in Surface Scattering Modeling

The physical picture of scattering and reflection of acoustic waves from the ocean surface is a stochastically random process, both in space and time. Fundamentally, analyses of this problem can be formulated from either the differential-equation or integral-equation statement of the problem. From the integral-equation formulation, one can single out the effects on the sound field due to the ocean surface; while the solution to the differential-equation statement of the problem, in principle, is more complete but it is less separable since scattering and/or reflection is included as part of a boundary-dependent propagation solution. As implied from the stated purposes of this study, subsequent discussions will be primarily concerned with the integral-equation framework.

In evaluating different methodologies of solving the surface scattering problem, a general consideration involves identification of the type of boundary description for the ocean surface. Exact analytical solutions are possible when one treats the ocean surface as a periodically rough surface. The most general statement of this problem specifies the ocean surface as a completely stochastic ensemble of propagating sinusoidal waves spanning the entire frequency spectrum. In some cases, the problem is simplified somewhat by eliminating the time dependence and assuming the ocean surface as a randomly rough frozen surface. Excluding the case of periodically rough surfaces, this study will consider the randomly rough surface and will specify whether it is a static or dynamic one for the methodology under consideration.

In addition to the boundary description, other general considerations that are needed in the process of assessing alternative methodologies, are associated with the chosen geometry of source and receiver as well as the fundamental characteristics of the water medium. Scattering solutions reported in the literature are normally tied to a specific source/receiver geometry. Since the intention is to incorporate a surface scattering submodel into a general procedure, this study will focus on the scattering cross-section solution, which describes the scattering intensity in each scattering direction per unit area per unit solid angle. For the same reason as well as the above-mentioned emphasis on the integral-equation formulation, effects due to propagation-related medium features will be considered in the total calculation, evaluated in the framework of RASP.

However, the most important consideration that helps to differentiate various methodologies rests with the fundamental approximation assumptions employed by each methodology. Implicitly implied from these assumptions will be the validity ranges of the solutions derived from the corresponding methodologies. It is therefore most natural to classify existing numerous solutions to the surface scattering problem principally on the basis of their fundamental approximation assumptions in combination with their solution approach. Discussions on various approximations are considerably facilitated through the use of several characteristic lengths associated with the problem. They can be identified as:

a, the rms surface waveheight;
λ, the acoustic wavelength; and
Λ, the ocean surface wavelength.

Even though one may assume that these approximations can all be translated into some well-defined mathematical statements involving only these three characteristic lengths, the task of examining various approximation schemes is yet further complicated by the fact that the same approximations are usually stated in different forms or implemented in different fashions. Therefore, at the expense of neglecting some of the more subtle aspects, the following discussions on alternative methodologies will be carried out in light of the two most often-used fundamental approximation assumptions. These are the small-waveheight and Kirchhoff approximations. They involve specific relationships between the above-mentioned characteristic lengths.

It should be noted at this point that there exists another fundamental approximation assumption that is widely made with regard to the time variation of the ocean surface. According to this assumption, the time variation of the ocean surface is relatively slow in comparison with the velocity of wave propagation. This quasistatic picture allows for a mathematically more manageable but reasonable description of the time-dependent scattered field. In dealing with the dynamic ocean surface, one would expect some variations in the spectrum of the scattered field relative to that of the incident field. This assumption then leads to an a priori observation that the scattered acoustic field will be a narrowband signal centered about the source frequency. As a result, this quasistatic approximation of the dynamic ocean surface is normally referred to as the narrow-band approximation.

The small-waveheight approximation is most often applied to the case where the slope and amplitude of the surface roughness are small. By this it is meant that the rms waveheight, a, is small compared with the acoustic wavelength λ and the minimum ocean surface wavelength Λ_{min} (Λ_{min} is associated with the maximum cut-off frequency of the ocean surface spectrum being considered). Mathematically, one writes this approximation as

$$a \ll \lambda \text{ and } a \ll \Lambda_{min} \ . \tag{2.1}$$

The Kirchhoff approximation is usually invoked when the scattered field at an observation point is written in the form of a Helmholtz integral using the half-space Green's function. This necessitates the knowledge of the first derivative of the scattered field at the interface, a quantity that is not readily available in the case of a randomly rough surface. The Kirchhoff approximation assumption then states that the required derivative is equal to the first derivative of the incident wave, which is a known quantity. The equivalence of this assumption is the statement that the ocean surface is "locally flat", or in terms of the chosen characteristic lengths,

$$\lambda \ll \Lambda_{min} \ . \tag{2.2}$$

In examining the connection between the small-waveheight and Kirchhoff approximations, Labianca and Harper [C1] pointed out that in several existing solutions, the Kirchhoff approximation is applied in conjunction with the small-waveheight one. In such cases, the validity domain is specified by

$$a \ll \lambda \ll \Lambda_{min} \ , \tag{2.3}$$

and, in fact, is contained within an overlapping region, that represents the limit $a/\lambda \to 0$ for the Kirchnoff approximation and $\lambda/\Lambda \to 0$ for the small-waveheight approximation. The domains of validity of these two approximation schemes together with their overlapping region are illustrated by a Venn diagram in Fig. 1. In this report, the major methodologies are examined in Appendices A through D with regard to their assumptions, formulation, and fundamental results. In reference to Fig. 1, one can readily recognize that all perturbation method solutions are valid in region A. Nevertheless, most of the considered Kirchhoff solutions are restricted to the overlapping region C instead of region B and their utility is therefore relatively limited. On the other hand, the composite-roughness solutions, in principle, is valid throughout the entire acoustic frequency span and, with a judicial separation of large-scale and small-scale portions of the ocean surface, it should be practically valid for any frequency range of interest. For the acoustic frequencies that range from very low to medium values, the solutions derived by the perturbation method and composite-roughness approach are probably more appropriate for use.

3. Relevance to NRL Reverberation Model RASP

In the preceding sections and attached Appendices, we have summarized and assessed a number of theoretical solutions to the problem of sound scattering from ocean surface. It is our desire to direct our immediate efforts to satisfy the need of reverberation prediction for the AAUS program. Consequently, our selection of scattering theories and what to do with them will be guided by the following requirements: first, the selected scattering submodels must be practically implementable and preferably compatible with the structure of the current NRL reverberation model, RASP; second, the resulting computational tools should be able to simulate as closely as possible the actual complex environmental conditions; and finally, order of preference should go in tandem with planned field experiments.

The first requirement implies that our effort should be focused on single-scatter models which are readily incorporated as addressable components of the RASP executive to describe elemental encounters with the ocean surface. The second calls for an adequate description of the ocean surface, of which some forms of solution can take advantage of but others cannot. This feature is required to further enhance forecasting capability by including annual and short term projections based upon actual environmental conditions, spatially varying sound velocity data, and detailed bathymetric data. Finally, the last requirement suggests that scattering models operational in the low-frequency and low-grazing angle ranges will be preferred. In addition, this requirement also demands that we should first concentrate on investigation of variation in surface reverberation due to changes in environmental parameters, such as wind speed and wind direction, before studying aspects of surface reverberation such as frequency spreading/shifting and temporal/spatial coherence, some of which are under investigation elsewhere.

In view of the above guidelines, the tangent plane method solutions examined in Appendix A appear not to address the frequency range of interest due to their underlining Kirchhoff assumption, which requires the acoustic wavelength be much smaller than the surface wavelength. In anticipation of this implication of the Kirchhoff approximation, we have specifically examined the low-frequency versions of these tangent plane method solutions, which were called "long-wave" by Eckart and "slightly-rough" by Parkins. Reduction to this special case, indeed, was achieved via an additional approximation that the surface wave height is much smaller than the acoustic wavelength, not to mention the introduction of the small-slope assumption into Eckart's solution. As a result, the use of these additional approximations in this case ultimately narrows considerably their validity domains. A more rigorous solution which was also based on the Kirchhoff approximation was developed by Tung, who did not use the small-slope assumption and replaced the Fraunhoffer approximation with the Fresnel one. His solution has led to many significant physical insights, especially those on the spectral distribution of the scattered field. However, quantitatively, the form of his solution was derived specifically for a rather simplistic analytical model of the surface wave spectrum and generally cannot accept as input a more practical surface spectrum model as required in the present study. Because of the above-mentioned reasons, none of the tangent plane method solutions examined in this report appears suitable.

In Appendix B we have closely examined three approaches to solving the surface scattering problem using the perturbation method. The fundamental assumption underlining this method is the small-waveheight approximation, which implies that the rms waveheight is much smaller than both the acoustic and surface wavelengths. Their domains of validity therefore coincide with the low-frequency range of our interest. A common feature of these solutions is that they all consist of two components, one describing the specular reflection and the other depicting scattering in all other directions. Most authors chose to examine in detail the scattered field except Kuperman who focused mainly on the specularly reflected component. The choice of which solution to be used in this class of solutions is greatly facilitated due to the fact that the solutions examined, although derived within different theoretical formulations, agree with each other except for a few nonessential details. Furthermore, we will be primarily concerned with the far-field solutions, which are what we need for combining with a ray-theoretic framework. In view of the above observations, it is clear that a well-established solution based on the first-order perturbation method exists and would satisfy our interest in the range of low frequencies. Another attractive aspect of this solution is that it provides an adequate description of surface scattering up to the first order in three spatial dimensions as well as frequency domain. As a consequence, the perturbation method solution as represented by Eqs. (B.30) and (B.53) is recommended for use in RASP.

At freqencies greater than a few hundred hertz the ratio of rms surface height to acoustic wavelength can become significant due to the large amplitude of the very long surface waves. The Kirchoff solution is adequate for the description of scattering from large gently undulating waves but is not adequate for the treatment of the diffractive scattering induced by the small amplitude short wavelength component of the surface roughness. The composite roughness model (Appendix C) treats the effect of the small scale roughness as a perturbation of the Kirchoff scattering from the large scale roughness. This extension of perturbation theory greatly exends the domain of validity of the perturbation approach. The theory's most serious limitations occur at very low grazing angles where the Kirchoff component of the approximation requires corrections for shadowing. The composite roughness submodel is summarized by Eqs. (C.6) and (C.28). This submodel should be used with caution so that the rms slope of the large scale roughness of the specified ocean surface is not on the order of the relevant grazing angles.

Another group of surface scattering descriptions reviewed in Appendix D were constructed by the empirical modeling approach on the basis of available experimental data. They represent empirical fittings of fairly comprehensive sets of scattering/reverberation acoustic and optic data. In the case of the Chapman-Harris and Martin backscattering models, their empirical formulae have been used extensively and have proved to be relatively accurate within their intended ranges of frequencies, grazing angles, and wind speeds. Their utility is nevertheless quite limited since they only describe the incoherent scattering strength for the backscattering geometry. Application of the empirical models thus cannot be extended to general scattering geometries and spectral analysis. However, because of the fact that they were worked out from field data, they are attractive in many aspects for comparison with other surface scattering models. RASP already includes the Chapman-Harris model and the Martin model will be incorporated later.

So far our selection of surface scattering submodels has included solutions by the first-order perturbation method and the composite-roughness approach and empirical formulas proposed by Chapman-Harris and Martin. There exist other physical mechanisms that would modify the scattered field but were not accounted for by these solutions. Among them, the two most important ones are bubble scattering at low grazing angles and shadowing effect associated with large-scale roughness and low grazing angles. Since these two effects can be analyzed separately and incorporated additionally to any surface scattering solutions, we intend to build them into RASP as two secondary options which can be combined with any of the selected surface scattering submodels.

As indicated at the beginning in Section 1, the performance quality of any surface scattering submodels critically depends on the quality of the ocean surface description in use. Specifically, one needs to have as inputs to these submodels reliable two-dimensional spectra of the surface wave amplitude and slope. We therefore have proceeded to review major modeling efforts for the ocean surface waves and have come to the conclusion that the best available two-dimensional surface wave spectrum would be a combination of the one-dimensional spectrum developed by Pierson [K4] and the azimuthal distribution proposed by Mitsuyasu [K6]. This combined surface wave spectrum is essential for use in the surface scattering submodel. In Appendix E, this combined model is reviewed and illustrated with sample computed spectra of surface waves.

In the following section, the recommended solutions of scattering cross-sections will be computed with the use of the above ocean surface model. Sample computations will be presented to illustrate the major features of these solutions and their variations with key environmental parameters.

4. Example Computations

On the basis of the assessment of different surface scattering solutions performed in the preceding sections and attached Appendices, we have reached the recommendation that the first-order perturbation method, composite-roughness approach and Chapman-Harris empirical model be used for computation of the surface scattering strength. In addition, as the most important environmental input, the two-dimensional surface spectrum modeled after a combination of the six-range Pierson's one-dimensional spectrum and the Mitsuyasu azimuthal dependence function will be employed in these computations whenever applicable. The objective of this section is then to illlustrate the computational results that can be achieved by the recommended solutions.

From the first-order perturbation method, the scattering cross section σ_{PM} is given by (see Eq. (E.30) of Appendix E)

$$\sigma_{PM}(\vec{\kappa},\omega) = 2k_{iz}^2 k_{sz}^2 \left[S_2(\vec{\kappa})\,\delta(\omega-\omega_o-\Omega)+S_2(-\vec{\kappa})\,\delta(\omega-\omega_o+\Omega)\right], \tag{4.1}$$

where S_2 is the two-dimensional surface wave spectrum. Other symbols used in Eq. (4.1) are defined as follows:

$\vec{k}_i$ = Incident wave vector,
$\vec{k}_s$ = Scattering wave vector,
w_o = Carrier frequency, and

$\vec{\kappa}$ and Ω are the resonant scattering wave vector and its corresponding Doppler-shifted frequency to be specified as

$$\vec{\kappa} = \vec{k}_{s\perp} - \vec{k}_{i\perp}, \tag{4.2}$$

$$\Omega = (g|\vec{\kappa}|)^{1/2}. \tag{4.3}$$

In the backscattering case, i.e. $\vec{k}_s = -\vec{k}_i$, Eq. (4.1) is reduced to

$$\sigma_{PM}(\vec{k}_s,\omega) = 2k_{sz}^4 \left[S_2(2\vec{k}_{s\perp})\,\delta(\omega-\omega_o-\Omega)+S_2(-2\vec{k}_{s\perp})\,\delta(\omega-\omega_o+\Omega)\right]. \tag{4.4}$$

We now want to examine several sample computations of the scattering cross section with the use of Eq. (4.4). In order to isolate the effect of wind speed variation, the azimuthal dependence of S_2 is removed by replacing it with an isotropic two-dimensional surface spectrum S_2^* defined by

$$S_2^*(\vec{\kappa}) = \frac{1}{2\pi} S_1(\vec{\kappa}), \tag{4.5}$$

where S_1 is the Pierson's one-dimensional spectrum presented in Appendix E.

Figures 2a and 2b present the variation of the isotropic backscattering cross section with respect to representative values of the wind speed at two acoustic frequencies, 200 Hz and 50 Hz, respectively. In the 200 Hz case, the variation of σ_{PM} with wind speed appears minimal (less than 5 dB) for all grazing angles, except for those angles higher than 60°. This is mainly influenced by the fact that at 200 Hz the resonant scattering frequency,

$$\Omega = (2g|\vec{k}_{s\perp}|)^{1/2}, \tag{4.6}$$

varies from 0.65 Hz to 0.25 Hz as the grazing angle increases from 0° to 70°. In this frequency range of surface waves, it is seen from Fig. E2 that the spectral level does not vary considerably with the wind speed. At the lower acoustic frequency, 50 Hz, Fig. 2b shows that that variation of the isotropic backscattering cross section with respect to wind speeds is more significant, especially between 3.5 m/s and 7.4 m/s. This characteristic again can be related to the surface spectrum, where the spectral level is seen to vary considerably in the frequency window 0.12 - 0.32 Hz, representing the variation of the resonant scattering frequencies in the same grazing angle range.

With regard to the composite-roughness approach, the general functional behavior of the scattering cross section is similar to that of the perturbation method, except for the tilting effect that modifies the effective grazing angle. Its scattering cross section can be written as (see Eqs. (C.6) and (C.28))

$$\begin{aligned}\sigma_{CR}(\theta_i,\theta_s,\omega) = {} & 2k_c^4 \sin^2(\theta_i+\Delta\theta)\sin^2(\theta_s+\Delta\theta) \\ & \cdot[S_2(\vec{K})\delta(\omega-\omega_0-\Omega)+S_2(-\vec{K})\delta(\omega-\omega_0+\Omega)],\end{aligned} \tag{4.7}$$

in which

$$\begin{aligned}\Delta\theta &= -\frac{S_\theta}{2}+\frac{1}{2}\left\{S_\theta^2-4P_\theta+4\left[P_\theta^2+\epsilon_{rms}^2(S_\theta^2+2P_\theta)+3\epsilon_{rms}^4\right]^{1/2}\right\}^{1/2}, \\ S_\theta &= \theta_i+\theta_s, \\ P_\theta &= \theta_i\theta_s,\end{aligned} \tag{4.8}$$

where θ_i and θ_s are the grazing and scattering angles, ϵ_{rms} the rms slope of surface waves, and other symbols are defined as before. The above-mentioned tilting effect is embodied in the quantity $\Delta\theta$ of Eq. (4.7).

In the case of backscattering, Eqs. (4.7) and (4.8) are simplified to

$$\begin{aligned}\sigma_{CR}(\theta_s,\omega) = {} & 2k_s^4\sin^4(\theta_s+\Delta\theta) \\ & \cdot[S_2(\vec{K})\delta(\omega-\omega_0-\Omega)+S_2(-\vec{K})\delta(\omega-\omega_0+\Omega)],\end{aligned} \tag{4.9}$$

in which

$$\Delta\theta = (\theta_s^4+6\epsilon_{rms}^2\theta_s^2+3\epsilon_{rms}^4)^{1/4}-\theta_s. \tag{4.10}$$

Again, we compute and present in Fig. 3 the isotropic backscattering cross section as derived by the composite-roughness approach for different wind speeds at the acoustic frequency of 200 Hz. Variation with the wind speed is seen not to be considerable. In this particular set of calculations, we also include a computation that uses the familiar Phillips spectrum as input instead of our adapted Pierson's spectrum. The resulting difference is obvious as indicated in Fig. 2, which demonstrates the criticality of which surface spectrum model to be used as input in theoretical prediction of the surface scattering cross section.

The above two surface scattering theories together with the Chapman-Harris empirical model (see Appendix D) are now compared using the same acoustic and environmental parameters. Figure 4 presents the isotropic backscattering cross section computed by these three models for acoustic frequency of 200 Hz and wind speed of 3.5 m/s. At high grazing angles, e.g. larger than 50°, their predictions are very similar. However, as the grazing angle becomes small, their predictions begin to deviate from each other. Chapman-Harris model's prediction is about at least 10 dB consistently lower than those of the other two solutions. Among the perturbation method and composite-roughness approach, the scattering strength predicted by the latter approaches a low but finite level at about -70 dB for grazing angles of a few degrees, while the former practically predicts no backscattered energy. In general, the difference between the perturbation method and composite-roughness approach is only significant for grazing angles less than 20°.

In the above computations, we have removed the azimuthal dependence of the surface scattering cross section and, as a consequence, effectively incoherently summed the two constituent Doppler-shifted components. Utilization of the proper two-dimensional surface spectrum instead of Eq. (4.5) would enable us to resolve these two components and examine the effect of the wind direction upon their respective strengths. In Figs. 5a through 5d, the two-dimensional surface spectrum developed in Appendix E is employed to evaluate the backscattering strength of both the up-shifted and down-shifted frequency components for different wind directions but the same wind speed. As the wind direction is changed from almost cross-wind (Fig. 5a) to up-wind (Fig. 5d), the down-shifted component slowly gains strength while the up-shifted component quickly loses its intensity. For the cross-wind condition, the two components are expected to be equal in strength and for the up-wind condition only the down-shfited component exists.

Indeed, other than the backscattering case, the perturbation method as described by Eq. (4.1) can predict the surface scattering cross section for all scattering directions, both in and out of the plane of incidence. In this regard, the composite-roughness solution as represented by Eq. (4.7) is able to describe the scattering cross section for all directions in the plane of incidence. These capabilities are demonstrated in Figs. 6 and 7, where the incoherent (up-shifted plus down-shifted) scattering strength is plotted versus the scattering angle in the plane of incidence for a given grazing angle. The computations presented in Fig. 6 are performed for wind speed of 3.5 m/s, acoustic frequency 200 Hz, grazing angle 30°, and two wind directions

(up-wind and cross-wind), employing both perturbation and composite-roughness solutions. Similar computations are presented in Fig. 7 using the same parametric values except for a different wind speed, 7.4 m/s. The following observations can be drawn from these two figures: (i) At low wind speed, 3.5 m/s, the scattering strengths vary considerably with the wind direction; (ii) At moderate wind speed, 7.4 m/s, and at acoustic frequency of 200 Hz, the wind direction has a significant effect on the predicted scattering strength only in the forward-scattered directions; and (iii) Difference between the perturbation and composite-roughness solutions is noticeable only for scattering angles in the neighborhood of 0° and 180°.

5. Conclusions and Future Developments

Assessment of various theoretical formulations and examination of their principal results in this report has led to an appropriate selection of alternative surface scattering submodels and associated surface wave spectra that would be most compatible with AAUS interests as well as the current NRL reverberation prediction model, RASP. The requirements of low- to mid-range frequencies and low grazing angles represent the driving rationale for us to adapt the following approach to modeling surface scattering in our current effort in reverberation prediction:

(i) Two theoretical formulations, the first-order perturbation method and the composite-roughness approach, are selected to be incorporated into RASP. The composite-roughness solution would warrant a broader coverage of the frequencies of interest. The principal differences between these two solutions are two-fold: First, near 0° or 180° scattering angles the composite-roughness solution approaches a finite value for scattering strength while the perturbation method leads to an infinitely small scattering strength; and second, at the present stage the composite-roughness approach can describe the scattering cross section in the plane of incidence whereas the perturbation solution is capable of depicting the scattering strength in all three-dimensional directions. (One reason to incorporate the perturbation solution is due to the anticipation of the eventual consideration of three-dimensional effects in the reverberation problem.)

(ii) Two backscattering empirical models, Chapman-Harris and Martin, will also be introduced into RASP. As well-established empirical formulae, they will serve as useful double-check options and will be used as bases for future additions of new field measurements into an empirical fitting framework as needs arise.

(iii) The two-dimensional surface wave spectrum modeled from a combination of the six-range Pierson one-dimensional spectrum and the azimuthal distribution proposed by Mitsuyasu et al. appears to be the most realistic and comprehensive empirical description based on available information at the present time. In addition, the choice of this combined spectrum is also motivated by the fact that it adequately meets the input requirement of most existing surface scattering formulations and its fitting algorithms are flexible enough to accommodate new ocean surface measurements, which are being acquired in the present experimental plan of the AAUS program.

At the completion of this study, our effort in investigating surface reverberation has by no means reached the desired understanding. Future research efforts are therefore proposed to be pursued in the following directions:

(i) It is obvious that the next step would be to implement the above recommended surface scattering options in RASP. This can be achieved with some minor modifications to the present programming code of RASP.

(ii) Our understanding of the reverberation intensity would be solidified as the result of the above efforts. However, there exists a strong need to also characterize the spectral content of the surface reverberation signal. It is therefore desirable to speed up investigation of the problem of frequency shifting and spreading for surface reverberation. Due to the rather immediate need of this understanding, investigation of this problem should be simultaneously pursued in two directions, both independently of RASP and within the ray-theoretic framework of RASP.

(iii) Finally, in a more long-term time frame, the stochastic fluctuations of the ocean surface environment which would obviously degrade the reverberation signal must be addressed to enhance our prediction capabilities. This implies that we will have to investigate the amplitude and phase fluctuations of the surface scattering field and consequently can estimate the critical concepts of temporal and spatial coherence of the surface reverberation signal.

Bibliography

A. Review:

1. L. Fortuin, "Survey of literature on reflection and scattering of sound waves at the sea surface," J. Acoust. Soc. Am. 47, 1209 (1970).

2. H. Trinkaus, "Fundamental approximations for the scattering of acoustic waves from a rough surface, "SACLANT ASW Research Center Memorandum SM-15, La Spezia, Italy (1973).

3. L. Brekhovskikh and Y. Lysanov, "Fundamentals of Ocean Acoustics," Springer-Verlag, New York (1982).

4. F. G. Bass and I. M. Fuks, "Wave scattering from statistically rough surfaces," Pergamon Press, New York (1979).

5. A. Ishimaru, "Wave propagation and scattering in random media: Volumes 1 and 2," Academic Press, New York (1978).

B. Tangent Plane Method:

1. D. M. F. Chapman, "An improved Kirchhoff formula for reflection loss at a rough ocean surface at low grazing angles," J. Acoust. Soc. Am. 73, 520 (1983).

2. L. J. Ziomek, "Generalized Kirchhoff approach to the ocean surface-scatter communication channel. Part I: Transfer function of the ocean surface," J. Acoust. Soc. Am. 71, 116 (1982).

3. L. J. Ziomek, "Generalized Kirchhoff approach to the ocean surface-scatter communication channel. Part II: Second-order functions," J. Acoust. Am. 71, 1487 (1982).

4. H. Tung, "Frequency spreading in underwater acoustic signal transmission," Ph. D. Thesis, Department of Engineering and Applied Science, Yale University (1980).

5. B. E. Parkins, "Scattering from the time-varying surface of the ocean," J. Acoust. Soc. Am. 42, 1262 (1967).

6. W. C. Meecham, "On the use of the Kirchhoff approximation for the solution of reflection problems," J. Rational Mech. Anal. 5, 325 (1956).

7. C. Eckart, "The scattering of sound from the sea surface," J. Acoust. Soc. Am. 25, 566 (1953).

C. Perturbation Method

1. F. M. Labianca and E. Y. Harper, "Connection between various small-waveheight solutions of the problem of scattering from the ocean surface," J. Acoust. Soc. Am. 62, 1144 (1977).

2. F. M. Labianca and E. Y. Harper, "Sideband structure of sound from a harmonic point source scattered by a rough surface moving over an upward-refracting ocean," J. Acoust. Soc. Am. 61, 378 (1977).

3. F. M. Labianca and E. Y. Harper, "Asymtotic theory of scattering by a rough surface progressing over an inhomogeneous ocean," J. Acoust. Soc. Am. 59, 799 (1976).

4. E. Y. Harper and F. M. Labianca, "Scattering of sound from a point source by a rough surface progressing over an isovelocity ocean," J. Acoust. Soc. Am. 58, 349 (1975).

5. E. Y. Harper and F. M. Labianca, "Perturbation theory for scattering of sound from a point source by a moving rough surface in the presence of refraction," J. Acoust. Soc. Am. 57, 1044 (1975).

6. W. A. Kuperman, "On scattering from a moving rough surface without a Kirchhoff or a farfield approximation," J. Acoust. Soc. Am. 64, 1113 (1978).

7. W. A. Kuperman and F. Ingenito, "Attenuation of the coherent component of sound propagating in shallow water with rough boundaries," J. Acoust. Soc. Am. 61, 1178 (1977).

8. W. A. Kuperman, "Coherent component of specular reflection and transmission at a randomly rough two-fluid interface," J. Acoust. Soc. Am. 58, 365 (1975).

9. F. G. Bass, V. D. Freulicher, and I. M. Fuks, "Propagation in statistically irregular waveguides- PartI: Average field," IEEE Trans. AP-22, 278 (1974).

10. F. G. Bass, V. D. Freulicher, and I. M. Fuks, "Propagation in statiscally irregular waveguides- Part II: Second-order statistical moments," IEEE Trans. AP-22, 288 (1974).

11. Lord Rayleigh (J. W. Strult), "The theory of sound," Dover, New York, 89-96, (1945).

12. R. F. Millar, "The Rayleigh hypothesis and a related least-squares solution to scattering problems for periodic surfaces and other scatters," Radio Science 8, 785 (1973).

13. H. W. Marsh, "Sound reflection and scattering from the sea surface," J. Acoust. Soc. Am. 35, 240 (1963).

14. H. W. Marsh, "Nonspecular scattering of underwater sound by the sea surface," in "Underwater acoustics: Proceedings of the NATO Institute at Imperial College," (ed. V. M. Albers) Plenum Press, New York (1962).

15. H. W. Marsh, "Scattering of underwater sound by the sea surface," J. Acoust. Soc. Am. 33, 334 (1961).

16. H. W. Marsh, "Exact solution of wave scattering by irregular surfaces," J. Acoust. Soc. Am. 33, 330 (1961).

17. E. Y. T. Kuo, "Wave scattering and transmission at irregular surfaces," J. Acoust. Soc. Am. 36, 2135 (1964).

D. Composite-roughness Approach

1. W. Bachmann, "A theoretical model for the backscattering strength of a composite-roughness sea surface," J. Acoust. Soc. Am. 54, 712 (1973).

2. S. T. McDaniel and A. D. Gorman, "Analysis of acoustic and radar sea-surface reverberation using the composite-roughness model," Technical Memorandum 81-106, Applied Research Laboratory, the Pennsylvania State University, Pennsyvania (1981).

3. S. T. McDaniel and A. D. Gorman, "An examination of the composite-roughness scattering model," J. Acoust. Soc. Am. 73, 1496 (1983).

E. Empirical Modeling

1. J. J. Martin, "Acoustic reverberation at the sea surface: surface and sublayer spectra vis-à-vis scattering and reflection," U. S. Navy J. *Underwater Acoustics* 20, 505 (1970).

2. J. J. Martin, "Sea surface roughness and acoustic reverberation- An operational model," J. Acoust. Soc. Am. 40, 697 (1966).

3. R. P. Chapman and H. D. Scott, "Surface backscattering strengths measured over an extended range of frequencies and grazing angles," J. Acoust. Soc. Am. 36, 1735 (1964).

4. R. P. Chapman and J. H. Harris, "Surface backscattering strengths measured with explosive sound sources," J. Acoust. Soc. Am. 34, 1592 (1962).

F. Scattering from Subsurface Bubbles

1. J. C. Novarini and D. R. Bruno, "Effects of the subsurface bubble layer on sound propagation," J. Acoust. Soc. Am. 72, 510 (1982).

2. D. R. Bruno and J. C. Novarini, "Coherence and multiple scattering effects on acoustic backscattering from linear arrays of gas-filled bubbles," J. Acoust. Soc. Am. 71, 1359 (1982).

3. P. A. Crowther, "Acoustical scattering from near-surface bubble layers," in " Cavitation and Inhomogeneities in Underwater Acoustics," (ed. W. Lauterborn), Springer-Verlag, New York (1980).

4. H. Medwin, "The rough surface and bubble effects on sound propagation in a surface duct," Report NPS- 61Md71101A, Physics Department, U. S. Naval Postgraduate School, Monterey, California (1971).

G. Shadowing Effects

1. B. G. Smith, "Geometrical shadowing of a random rough surface," IEEE Trans. AP-15, 668 (1967).

2. R. J. Wagner, "Shadowing of randomly rough surfaces," J. Acoust. Soc. Am. 41, 138,(1967).

3. P. Beckmann, "Shadowing of random rough surfaces,"Trans. IEEE AP-13, 384 (1965).

H. Point-scatterer Quasiphenomenological Approach

1. G. R. Wilson and M. E. Frazer, "Horizontal covariance of surface reverberation: Comparison of a point-scatter model to experiment," J. Acoust. Soc. Am. 73, 749 (1983).

2. T. D. Plemons, J. A. Shooter, and D. Middleton, "Underwater acoustic scattering from lake surface, I. Theory, experiment, and validation of data," J. Acoust. Soc. Am. 52, 1487 (1972).

3. T. D. Plemons, J. A. Shooter, and D. Middleton, "Underwater acoustic scattering from lake surfaces. II. Covariance functions and related statistics," J. Acoust. Soc. Am. 52, 1503 (1972).

4. D. Middleton, "A statistical stheory of reverberation and similar first-order scattered fields. Part I: Waveform and the general process," IEEE Trans. IT-13, 372 (1967).

5. D. Middleton, "A statistical theory of reverberation and similar first-order scattered fields. Part II: Moments, spectra, and spatial distributions," IEEE Trans. IT-13, 393 (1967).

6. D. Middleton, "A statistical theory of reverberation and similar first-order scattered fields. Part III: Wavesforms and fields," IEEE Trans IT-18, 35 (1972).

7. D. Middleton, "A statistical theory of reverberation and similar first-order scattered fields. Part IV: Statistical models," IEEE Trans. IT-18, 68 (1972).

8. V. V. Ol'Shevskii, "Characteristics of sea reverberation," Consultants Bureau, Plenum, New York (1967).

I. Reflection and Diffraction

1. J. C. Novarini and H. Medwin, "Diffraction, reflection, and interference during near-grazing and near-normal ocean surface backscattering," J. Acoust. Soc. Am. 64, 260 (1978).

2. C. S. Clay and H. Medwin, "Acoustical Oceanography," Wiley, New York, Chapt. 10, (1977).

3. A. W. Trorey, "A simple theory for seismic diffractions," Geophysics 35, 762 (1970).

J. Propagation Modeling with Rough Surface Scattering

1. C. A. Boyles, "Coupled mode solution for cylindrically synmetric oceanic waveguide with a range and depth dependent refractive index and a time varying rough sea surface," J. Acoust. Soc. Am. 73, 800 (1983).

2. L. B. Dozier, "Numerical solution of coupled mode equations," Report SAI-83-808-WA, Science Applications, Inc., Virginia (1982).

3. L. B. Dozier, "PERUSE: A numerical treatment of rough surface scattering for the parabolic wave equation," Report SAI-82-436-WA, Science Applications, Inc., Virginia (1981).

4. S. T. McDaniel, "Comparison of coupled-mode theory with the small-waveheight approximation for sea-surface scattering," J. Acoust. Soc. Am. 70, 535 (1981).

5. A. Beilis and F. D. Tappert, "Coupled mode analysis of multiple rough surface scattering," J. Acoust. Soc. Am. 66, 811 (1979).

6. H. L. Wilson and F. D. Tappert, "Acoustic propagation in random oceans using the radiation transport equation," J. Acoust. Soc. Am. 66, 256 (1979).

K. Modeling of Ocean Surface Wave Spectra

1. J. A. Neubert, "State of the art in ocean-atmosphere interface modeling," Technical Report 809, Naval Ocean Systems Center, San Diego, California (1982).

2. T. T. Kadota and F. M. Labianca, "A mathematical representation of random gravity waves in the ocean," IEEE J. Oceanic Engineering OE-5, 215 (1980)

3. H. Mitsuyasu, "Measurement of the high-frequency spectrum of ocean surface waves," J. Physical Oceanography 7, 882 (1977).

4. W. J. Pierson, Jr., "The theory and applications of ocean wave measuring systems at and below the sea surface on the land, from aircraft and from spacecraft," Contractor Report CR-2646, NASA (1976).

5. K. Hasselmann, D. B. Ross, P. Müller and W. Sell, "A parametric wave prediction model," J. Physical Oceanography 6, 200 (1976).

6. H. Mitsuyasu, F. Tasai, T. Suhara, S. Mizuno, M. Ohkusu, T. Honda and K. Rikiishi, "Observations of the directional spectrum of ocean waves using a cloverleaf buoy," J. Physical Oceanography 5, 750 (1975).

7. T. P. Barnett and K. E. Kenyon, "Recent advances in the study of wind waves," Rep. Prog. Phys. 38, 667 (1975).

8. G. L. Tyler, C. C. Teague, R. H. Stewart, A. M. Peterson, W. H. Munk and J. W. Joy, "Wave directional spectra from synthetic aperture observations of radio scatter," Deep-Sea Research 21, 989 (1974).

9. W. J. Pierson, Jr. and R. A. Stacy, "The elevation, slope and curvature spectra of a wind roughened sea surface," Contractor Report CR-2247, NASA (1973).

10. L. Moskowitz, "Estimates of the power spectrums for fully developed seas for wind speeds of 20 to 40 knots," J. Geophysical Research 69, 5161 (1964).

11. W. J. Pierson, Jr. and L. Moskowitz, "A proposed spectral form for fully developed wind seas based on the similarity theory of S. A. Kitaigorodskii," J. Geophysical Research 69, 5181 (1964).

12. W. J. Pierson, Jr., "The interpretation of wave spectrums in terms of the wind profile instead of the wind measured at a constant height," J. Geophysical Research 69, 5191 (1964).

13. C. Cox and W. Munk, "Measurement of the roughness of the sea surface from photographs of the sun's glitter," J. Opt. Soc. Am. 44, 838 (1954).

14. O. M. Phillips, "The dynamics of the upper ocean," Cambridge University Press, London (1966).

15. V. J. Cardone, "Specification of the wind field distribution in the marine boundary layer for wave forecasting," Geophysical Sciences Laboratory Report TR-69-1, New York University, 1969.

APPENDIX A

Tangent Plane Method

In general, application of the Kirchhoff approximation to the problem of acoustic scattering from the ocean surface was normally done within the context of the Helmholtz integral over a half-space integration contour. Eckart [B7] employed this formulation to investigate scattering from a frozen randomly rough surface. Later, Parkins [B5] extended Eckart's analysis to include the time variation of the ocean surface, i.e., to the case of a dynamic stochastic surface. Recently, this method of solution was further refined by Tung [B4] to improve its accuracy and to account for wave-slope statistics and a more general source/receiver geometry. In addition to these major works, several other authors [C1-C3] attempted to develop ways to compensate for a major deficiency inherent in the Kirchhoff approximation, caused by the so-called shadowing effect. In this Appendix, we will summarize and discuss the major solutions that are based on the Kirchhoff approximation scheme. Since there have been numerous studies using this approach, following discussions on this methodology will have to be focused on the works of only several key researchers. Attempts will be made to recast these works in the same terminology for them to be comparable.

A1. Eckart

The problem investigated by Eckart [B7] was to derive the scattering cross section for an acoustic point source. This was formulated from the half-space Helmholtz integral, which describes the scattered pressure field as

$$p_s(\vec{r}_s) = \frac{1}{4\pi} \iint_{\Sigma} \frac{e^{ikr_s}}{r_s} \frac{\partial p_s}{\partial \hat{n}} - p_s \frac{\partial}{\partial \hat{n}} \left(\frac{e^{ikr_s}}{r_s} \right) d\Sigma \qquad (A.1)$$

for an incident field of the form

$$p_i(\vec{r}_i) = P \frac{e^{ikr_i}}{r_i} . \qquad (A.2)$$

In Eqs. (A.1) and (A.2), P is the directional source amplitude; Σ is the ocean surface described by $z = \zeta(x,y,t)$; $\hat{n}$ is the unit vector normal to Σ; k is the acoustic wave number; and $\vec{r}_s$ and $\vec{r}_i$ are as illustrated in Fig. A1.

At this point, Eckart applied the pressure-release boundary condition and the Kirchhoff approximation at the surface,

$$p_i + p_s = 0 , \qquad (A.3)$$

$$\frac{\partial p_i}{\partial \hat{n}} = \frac{\partial p_s}{\partial \hat{n}} , \qquad (A.4)$$

to write Eq. (A.1) as

$$p_s(\vec{r}_s) = \frac{1}{4\pi} \iint_{\Sigma} \frac{\partial}{\partial \hat{n}} \left(p_i \frac{e^{ikr_s}}{r_s} \right) d\Sigma . \tag{A.5}$$

Equation (A.1) was then simplified further through the use of the following approximations;

(i) Fraunhoffer approximation:

$$\begin{aligned} r_i r_s &\simeq R_i R_s , \\ r_i + r_s &\simeq R_i + R_s + \vec{r} \cdot (\hat{R}_i - \hat{R}_s) ; \end{aligned} \tag{A.6}$$

(ii) Small-slope approximation:

$$\begin{aligned} \frac{\partial}{\partial \hat{n}} &\rightarrow \frac{\partial}{\partial z} , \\ d\Sigma &\rightarrow dx\,dy . \end{aligned} \tag{A.7}$$

The Fraunhoffer approximation is based on the assumption that both source and receiver are in the far field and the source beam pattern is highly directional. The small-slope approximation, which allows the integration to be carried out on the surface Σ_{xy}, the projection of Σ onto the (x,y) plane, implies that $a \ll \Lambda$. With these additional approximations, Eq. (A.5) becomes

$$p_s(\vec{r}_s) = -\frac{i\gamma k}{4\pi} \frac{e^{ik(R_s + R_i)}}{R_s R_i} \int_{\Sigma_{xy}} P(x,y) e^{-ik(\alpha x + \beta y + \gamma z)} dx\,dy , \tag{A.8}$$

where α, β, and γ are the Cartesian components of $(\hat{R}_s - \hat{R}_i)$. If we define $\vec{k}_i$ and $\vec{k}_s$ to be the incident and scattered wave vectors, respectively, then γk is the z-component of $\vec{K} = \vec{k}_s - \vec{k}_i$.

From Eq. (A.8), Eckart proceeded to study two simplified cases, which were called "long-wave" and "short-wave" in his terminology. Since the "short-wave" solution was derived for a specific form of the ocean surface spectrum and thus was not generally useful, we will discuss only the "long-wave" solution here. The "long-wave" case was prescribed by the following approximation

$$e^{-i\gamma k z} \simeq 1 - i\gamma k z , \tag{A.9}$$

which leads to the condition

$$\frac{2\pi\gamma z}{\lambda} \ll 1 \quad \text{or} \quad a \ll \lambda . \tag{A.10}$$

Writing the intensity of the scattered field from Eq. (A.8) in terms of the spatial covariance function of the surface wave height,

$$\Phi_s(x', y'; x'', y'') = \langle \mathcal{Z}(x', y', t)\, \mathcal{Z}(x'', y'', t) \rangle , \tag{A.11}$$

Eckart derived the scattering cross section per unit solid angle per unit area as

$$\sigma_{sc} = \left(\frac{K_z^2}{4\pi}\right)^2 S_s(K_x, K_y) , \tag{A.12}$$

where $S_s(K_x, K_y)$ is the spatial two-dimensional spectrum of the ocean surface waves, which is defined by

$$S_s(K_x, K_y) = \iint \Phi_s(\xi, \eta)\, e^{-i(\xi K_x + \eta K_y)}\, d\xi\, d\eta \tag{A.13}$$

for a homogeneous ocean surface $(\xi = x'' - x', \eta = y'' - y')$.

A2. Parkins

The problem studied by Parkins [B5] differs from that by Eckart in two aspects: An incident plane wave was considered instead of a point source and time variation of the ocean surface was included in Parkins' treatment. Parkins' solution was developed from a half-space Helmholtz integral of a slightly different form, which was based on an impulse-type Green function [see J. A. Stratton, "Electromagnetic Theory," McGraw-Hill, New York, 1941, p. 427]. In our present notation, this integral can be written as

$$p_s(\vec{r}_s, t) = \frac{1}{4\pi} \iint_{\Sigma} \frac{1}{r_s} \left[\frac{\partial}{\partial \hat{n}} (p_i + p_s)\right] d\Sigma \tag{A.14}$$

for the incident field p_i given by

$$p_i(\vec{r}, t) = P_0\, e^{-i\vec{k}_i \cdot \vec{r}}\, e^{i\omega t} , \tag{A.15}$$

where P_0 is the amplitude of the incident plane wave and the square brackets denote time retardation. Because of considering an incident plane wave, Parkins could carry out the differentiation $\partial/\partial\hat{n}$ exactly without resorting to the small-slope approximation as Eckart did. This results in

$$\left[\frac{\partial}{\partial \hat{n}} (p_i + p_s)\right] = -2i(\hat{n} \cdot \vec{k}_i)\, e^{-i\vec{k}_i \cdot \vec{r}}\, e^{-ik_s r_s}\, e^{i\omega t} , \tag{A.16}$$

in which the Kirchhoff approximation has been applied and evaluation at the retarded time implemented.

Using Eq. (A.16) and the fact that

$$\hat{n} = (-z_x, z_y, 1)/(z_x^2 + z_y^2 + 1)^{1/2},$$
$$d\Sigma = (z_x^2 + z_y^2 + 1)^{1/2}\, dx\,dy, \tag{A.17}$$

Parkins transformed Eq. (A.14) into

$$p_s(\vec{r}_s, t) = \frac{iP_o e^{i\omega t}}{2\pi} \iint_{\Sigma_{xy}} \frac{e^{-i(k_s r_s + \vec{k}_i \cdot \vec{r})}}{r_s} \left(k_{ix} z_x + k_{iy} z_y - k_{iz}\right) dx\,dy. \tag{A.18}$$

At this point, Parkins invoked the far-field Fraunhoffer approximation in the form

$$r_s \simeq R_s \text{ in the denominator, and}$$
$$r_s \simeq R_s - \hat{R}_s \cdot \vec{r} = R_s - \hat{k}_s \cdot \vec{r} \text{ in the exponential,} \tag{A.19}$$

to obtain

$$p_s(\vec{r}_s, t) = \frac{iP_o e^{i(\omega t - k_s R_s)}}{2\pi R_s} \iint_{\Sigma_{xy}} e^{i\vec{K}\cdot\vec{r}} \left(k_{ix} z_x + k_{iy} z_y - k_{iz}\right) dx\,dy. \tag{A.20}$$

Through a simple integration by parts, Eq. (A.20) becomes

$$p_s(\vec{r}_s, t) = \frac{iP_o e^{i(\omega t - k_s R_s)}}{2\pi R_s} (\vec{K} \cdot \vec{k}_i) \iint_{\Sigma_{xy}} e^{i\vec{K}\cdot\vec{r}} \left(\frac{1}{K_z} - 2z\right) dx\,dy. \tag{A.21}$$

Now, Parkins made the assumption that "the aperture is many wavelengths across" [85, p. 1263] to obtain the following key result

$$p_s(\vec{r}_s, t) = \frac{iP_o e^{i(\omega t - k_s R_s)}}{2\pi R_s} \frac{\vec{K} \cdot \vec{k}_i}{K_z} \iint_{\Sigma_{xy}} e^{i\vec{K}\cdot\vec{r}}\, dx\,dy. \tag{A.22}$$

From Eq. (A.22) the spectral density of the scattered field can be formally derived from

$$\varphi(\Omega) = \int_{-\infty}^{\infty} \Psi(\tau)\, e^{i\Omega\tau}\, d\tau, \tag{A.23}$$

where the covariance function Ψ is defined by

$$\Psi(\tau) = \langle p_s(x, y, t)\, p_s^*(x', y', t+\tau) \rangle. \tag{A.24}$$

The averaging operation in Eq. (A.24) was considerably simplified by assuming that the joint distribution of the surface wave height is Gaussian. This then leads to

$$\Psi(\tau) = p_0 e^{-i\omega\tau} \iint_{\Sigma_{xy}} \iint_{\Sigma_{\xi\eta}} e^{-K_z^2\sigma^2[1-\Phi(\tau)]} e^{-i(K_x\xi + K_y\eta)} d\xi d\eta dx dy, \quad \text{(A.25)}$$

where

Φ = normalized covariance function of surface waveheight,

$\sigma^2 = \langle \zeta^2(x, y, t) \rangle$, and

$p_0 = (P_0/2\pi R_s)^2 (\vec{K} \cdot \vec{k}_i / K_z)^2$.

The spectral density of the scattered field was then solved explicitly for a special case, which was called "slightly rough surface" by Parkins. This was prescribed by the approximation

$$K_z^2\sigma^2 \ll 1 \quad \text{or} \quad a \ll \lambda,$$

leading to

$$e^{-K_z^2\sigma^2(1-\Phi)} \simeq e^{-K_z^2\sigma^2}(1 + K_z^2\sigma^2\Phi). \quad \text{(A.26)}$$

Considering the insonified area as a square of ($2\ell \times 2\ell$) dimension, Parkins showed from Eqs. (A.23), (A.25), and (A.26) that the scattering cross section per unit solid angle per unit area for the "slightly-rough" case had a coherent component $\sigma_{sc}^{(c)}$ and a Doppler-shifted component $\sigma_{sc}^{(d)}$ given as

$$\sigma_{sc}^{(c)}(\Omega) = \left(\frac{1}{\pi\ell}\right)^2 e^{-K_z^2\sigma^2} \left(\frac{\vec{K} \cdot \vec{k}_i}{K_z}\right)^2 \left(\frac{\sin K_x\ell \sin K_y\ell}{K_x K_y}\right)^2 \delta(\Omega - \omega), \quad \text{(A.27)}$$

$$\sigma_{sc}^{(d)}(\Omega) = \left(\frac{\vec{K} \cdot \vec{k}_i}{2\pi}\right)^2 e^{-K_z^2\sigma^2} S(K_x, K_y, \Omega - \omega), \quad \text{(A.28)}$$

where $S(K_x, K_y, \Omega)$ is the two-dimensional spectrum of surface waves defined by

$$S(K_x, K_y, \Omega') = \iiint_{-\infty}^{\infty} \Phi(\xi, \eta, \tau) e^{-i(K_x\xi + K_y\eta - \Omega'\tau)} d\xi d\eta d\tau. \quad \text{(A.29)}$$

A3. Tung

Tung [B4] generalized Eckart's solution to include the time variation of the ocean surface. This was achieved by starting also from Eq. (A.1) but the scattering pressure p_s and its normal direction in this equation was evaluated at the retarded time. A major improvement in terms of accuracy of Tung's solution was obtained by dropping both Fraunhoffer and small-slope approximations. In place of the Fraunhoffer approximation, Tung employed the more general Fresnel approximation. Gain in accuracy of the Fresnel approximation is attributed to the fact that the horizontal components are kept up to the second order.

This can be better illustrated as follows. Referring to Fig. A1, one can write the exact expression for r_s as

$$r_s = R_s \left(1 - \frac{2\vec{R}_s \cdot \vec{r}}{R_s^2} + \frac{r^2}{R_s^2}\right)^{1/2}, \tag{A.30}$$

from which the Fraunhoffer approximation is derived in the form (compare with Eq. (A.19))

$$r_s \simeq R_s - \hat{R}_s \cdot \vec{r},$$

where $\vec{r} = (x,y,Z)$. More generally, if one retains only the first-order terms in Z but keeps the x and y terms up to the second order, one obtains the Fresnel approximation. From Eq. (A.30), this approximation is described as

$$r_s \simeq R_s \left\{1 - \frac{1}{R_s^2}\left[\vec{R}_s \cdot \vec{r} + \frac{r_\perp^2 - (\vec{R}_s \cdot \vec{r}_\perp)^2}{2}\right]\right\}, \tag{A.31}$$

where $\vec{r}_\perp = (x, y, 0)$.

Tung also avoided the use of the small-slope approximation in handling the $\partial/\partial \hat{n}$ differentiation by solving the Helmholtz integral for a specific surface spectrum. This in turn considerably limits the usefulness of Tung's solution, especially when the employed form of the surface spectrum is fairly simplistic and completely ignores the dispersive character of ocean waves. This surface spectrum was represented by the covariance function

$$\Phi(\xi, \eta, \tau) = \exp\left(-\frac{\xi^2}{\Lambda_x^2} - \frac{\eta^2}{\Lambda_y^2} - \frac{\tau^2}{T_0^2}\right) \cos\left[K(\eta - c_s t)\right], \tag{A.32}$$

where Λ_x, Λ_y and T_0 are the correlation lengths with respect to the x, y, and t dimensions. Equation (A.32) indeed only represents a surface wave propagating in the y direction with a velocity c_s and wavenumber K.

With regard to the temporal distribution of the ocean waves, instead of assuming a joint Gaussian distribution like Parkins, Tung carried out the averaging operation on the basis of the assumption that the surface height is "approximately" Gaussian and is uncorrelated with the slope. This allowed Tung to establish that the slope statistics was one of several reasons that caused asymmetric sidebands in the scattered field.

In the final analysis, Tung's solution is more rigorous in the sense that it is based on the Kirchhoff approximation alone, doing away with the far-field Fraunhoffer and small-slope approximations. However, its application is quite limited because it cannot accept a general empirical or experimentally-measured surface wave spectrum.

A4. Shadowing Function

The validity of various solutions to the surface scattering problem based on the Kirchhoff approximation is also limited by not incorporating the fact that the surface is only partially illuminated due to the roughness. A proper accounting of the so-called shadowing effect would certainly improve the rigor of these solutions. The fundamental concepts to investigate the shadowing effect was first developed by Beckmann [G3] and further elucidated later by Wagner [G1]. According to Wagner, the probability that a point Z_1, with slope Z_1' of the rough surface is illuminated, can be solved from the differential equation

$$\frac{d}{dX}\left[H(\theta_i|Z_1,Z_1',X)\right] = -q(X)H(\theta_i|Z_1,Z_1',X)\ , \tag{A.33}$$

in which the spatial parameters are illustrated in Fig. A2, $H(\theta_i|Z_1,Z_1',X)$ is the probability that the surface $Z(X)$ does not cross the ray $Z = Z_1+X\tan\theta_i$ in $[0,X]$ and $q(X)d(X)$ is the probability that $Z(X)$ crosses $Z = Z_1+X\tan\theta_i$ in $[X,X+dX]$ provided $Z(X)$ does not cross $Z = Z_1+X\tan\theta_i$ in $[0,X]$.

The solution to Eq. (A.33) has the form

$$H(\theta_i|Z_1,Z_1',X) = \exp\left[-\int_0^X q(X')\,dX'\right]\ . \tag{A.34}$$

As $X \to 0$

$$\begin{aligned} H(\theta_i|Z_1,Z_1',X) &\to 0 \quad \text{if} \quad Z_1' > \tan\theta_i\ , \\ H(\theta_i|Z_1,Z_1',X) &\to 1 \quad \text{if} \quad Z_1' < \tan\theta_i\ , \end{aligned} \tag{A.35}$$

so that

$$H(\theta_i|Z_1,Z_1') = h(\tan\theta_i - Z_1')\exp\left[-\int_0^\infty q(X)\,dX\right]\ , \tag{A.36}$$

where h is the unit step function and $H(\theta_i|Z_1,Z_1')$ is the probability that the point Z_1 with slope Z_1' is illuminated. A shadowing function, which is defined as the ratio of illuminated to total areas of the surface, is then obtained by averaging over all possible values of surface height and slope,

$$H(\theta_i) = \iint_{-\infty}^{\infty} H(\theta_i|Z_1,Z_1')\, W(Z_1)\, W'(Z_1')\, dZ_1\, dZ_1' , \tag{A.37}$$

in which $W(Z_1)$ and $W'(Z_1')$ are the probability densities of surface height and slope, respectively.

At this point, Wagner employed the following approximation assumptions:

(i) $q(X)$ is independent of the specific values of Z_1 and Z_1'; and

(ii) The rough surface $z = Z(x)$ is a normally distributed stationary random process described by

$$W(Z_1)W'(Z_1') = \frac{1}{2\pi}\,\frac{1}{\sigma|\sigma'|}\exp\left(-\frac{Z_1^2}{2\sigma^2}-\frac{Z_1'^2}{2\sigma'^2}\right), \tag{A.38}$$

where σ and σ' are the rms surface height and slope. With these two assumptions, Wagner derived from Eq. (A.37) an explicit expression for the shadowing function as

$$H(\theta_i) = \frac{(1+\operatorname{erf} A)(1-e^{-2B})}{4B}, \tag{A.39}$$

where

$$A = \frac{\tan\theta_i}{\sqrt{2}\,|\sigma'|}, \qquad B = \frac{e^{-A^2} - \sqrt{\pi}\,A \operatorname{erfc} A}{4\sqrt{\pi}\,A} . \tag{A.40}$$

In the limiting case $A \ll 1$, or low grazing angles, it was shown that

$$H(\theta_i) = \sqrt{\pi}\,A = \sqrt{\frac{\pi}{2}}\,\frac{1}{|\sigma'|}\tan\theta_i . \tag{A.41}$$

For a general scattering geometry, the shadowing function in Eq. (A.39) can be generalized to describe the shadowing effect on both incident and scattered rays. The results shown by Wagner are dependent on the scattering angle θ_s as follows:

(i) $0 \le \theta_s \le \pi/2$:

$$H(\theta_i,\theta_s) = \frac{\{1-\exp[-2(B_i+B_s)]\}(\operatorname{erf} A_i + \operatorname{erf} A_s)}{4(B_i+B_s)}, \tag{A.42}$$

where the A's and B's are defined as in Eq. (A.40);

(ii) $\pi/2 \leq \theta_s \leq \pi - \theta_i$:

$$H(\theta_i, \theta_s) = H(\theta_i) \text{ ; and} \tag{A.43}$$

(iii) $\pi - \theta_i \leq \theta_s \leq \pi$

$$H(\theta_i, \theta_s) = H(\theta_s) \text{ .} \tag{A.44}$$

APPENDIX B

Small Perturbation Method

In Appendix A, we have reviewed several major solutions that are based on the Kirchhoff approximation. The methodology commonly employed in these solutions is usually referred to as the tangent plane method. Another equally significant class of solutions that are constructed on the basis of the small-waveheight approximation essentially follow the perturbation approach. According to this perturbation methodology, the pressure-release boundary condition at the randomly rough surface is transformed to a set of boundary conditions at the unperturbed surface as the scattered sound field is expressed as a sum of perturbation fields of various orders. Under these newly transformed boundary conditions, the scattered field is then solved either by the Fourier transform technique or through the Helmholtz integral.

This approach was originated by Rayleigh [C11] who employed the small-waveheight approximation to obtain a scattering solution for a periodically rough surface. Indeed, Rayleigh's solution did not use the perturbation procedure as such but was associated with this methodology because of its similar approximate boundary condition. Later, Marsh [C13-C16] attempted to obtain an exact solution for the problem of scattering from a frozen randomly rough surface through the use of Wiener's generalized harmonic analysis. However, the useful, explicit form of his solution was an approximate one, which turned out to be limited by the small-waveheight approximation. The rigorous perturbation procedure was eventually applied to the surface scattering problem by a group of authors (Brekhovskikh [A3], Bass and Fuks [A4], Kuperman [C6-C8], and Harper and Labianca [C1-C5]). Of these authors, on the basis of their solution procedures, they were seen to follow two distinct approaches and thus could be separated into two groups. The first group, including Brekhovskikh, Bass and Fuks, and Kuperman, described the sound field as consisting of a mean field and a perturbation field, and transformed the pressure-release boundary condition through a Taylor series expansion to a set of boundary conditions at the mean surface. Brekhovskikh and Kuperman then went on to solve the problem by the Fourier transform technique, which was also known as the spectral representation analysis; while Bass and Fuks employed the Green function technique to solve the Helmholtz integral. The second group, which was pioneered by Harper and Labianca, applied the perturbation procedure to the total field up to the second order, transformed the pressure-release boundary condition in a similar fashion, and solved for the scattered field within the framework of a normal-mode representation. This last step of Harper and Labianca's approach implies that they have recast the scattering problem into a propagation one, although not as completely as later authors [J1-J6] who obviously took the lead from them. In this section, we will therefore focus on the works of Marsh, Brekhovskikh, and Kuperman.

B1. Marsh

Consider an incident plane wave p_i and the scattered field p_s. The scattered field is then expressed by a plane wave representation of the form

$$p_s(\vec{r}_s) = \iint_{-\infty}^{\infty} e^{-i\vec{k}_s \cdot \vec{r}_s} \, dG(k_{sx}, k_{sy}) , \tag{B.1}$$

where $G(k_{sx},k_{sy})$ is the generalized spectrum of the scattered field. The pressure-release boundary condition at the rough surface, $p_i + p_s = 0$, can be written as

$$-e^{-i\vec{k}_i \cdot \vec{r}} = \iint_{-\infty}^{\infty} e^{-i\vec{k}_s \cdot \vec{r}} \, dG(k_{sx}, k_{sy}) . \tag{B.2}$$

Next, the generalized spectrum G is represented as a power series in σ, the rms surface height,

$$G(k_{sx}, k_{sy}) = \sum_{n=0}^{\infty} \sigma^n A_n(k_{sx}, k_{sy}) . \tag{B.3}$$

Substitution of Eq. (B.3) in to Eq. (B.2) and collection of terms of the same power in σ yield an infinite set of linear differential-integral equations that in principle can be solved for the coefficients A_n's. Each of these linear equations is of the form

$$\frac{(-ik_{iz}\bar{z})^m}{m!} e^{-i(xk_{ix}+yk_{iy})} + \iint_{-\infty}^{\infty} e^{-i(xk_{sx}+yk_{sy})} \sum_{n=0}^{m} \frac{(ik_{sz}\bar{z})^n}{n!} dA_{m-n} = 0 , \tag{B.4}$$

in which $\bar{z}$ is the normalized surface waveheight, $\bar{z} = z/\sigma$.

Marsh [C15] solved a set of equations represented by Eq. (B.4) for $m = 0$, 1, and 2 for dA_0, dA_1, and dA_2. Through Eqs. (B.1) and (B.3), the covariance function Ψ of the scattered field is established as

$$\begin{aligned} \Psi(x,y) = {} & e^{-i(xk_{ix}+yk_{iy})} \left[1 + 4k_{iz}^2 \Phi_s(x,y)\right] \\ & - 4k_{iz} \iint_{-\infty}^{\infty} k_{sz} S_s(k_{sx} - k_{ix}, k_{sy} - k_{iy}) \, dk_{sx} \, dk_{sy} , \end{aligned} \tag{B.5}$$

where Φ_s is the spatial covariance function and S_s the spatial spectrum of the surface waves. The Fourier transform of $\Psi(x,y)$ then provides the scattering kernel

$$M(k_{sx}, k_{sy}) = R\delta(K_x)\delta(K_y) + 4k_{iz}^2 S_s(K_x, K_y) , \tag{B.6}$$

where $\vec{K} = \vec{k}_s - \vec{k}_i$ as before and R representing the specular reflection intensity is given by

$$R = 1 - 4k_{iz} \iint k_{sz} S_s(k_{sx} - k_{ix}, k_{sy} - k_{iy})\, dk_{sx}\, dk_{sy} . \tag{B.7}$$

In Eq. (B.6), the scattering kernel $M(k_{sk}, k_{sy})$ describes the scattered intensity in the direction of $\vec{k}_s$.

B2. Brekhovskikh

As indicated earlier, there are several authors who essentially followed a similar perturbation approach. To save space and for the ease of comparative analysis, it is desirable to present their results in a common terminology despite the fact that each author focused on different aspects of the problem. Differences or similarities will be pointed out wherever appropriate. Brekhovskikh's analysis [A3, Chapter 9] of the problem of scattering from the ocean surface is probably the most succinct presentation and will therefore be discussed first.

B21. First-order Perturbation Field

The pressure-release boundary condition for the total field $p(\vec{r})$ at the rough surface $z = Z(x,y)$ is expanded into a Taylor series up to the first order in Z,

$$p + Z \frac{\partial p}{\partial z} = 0 \quad \text{at} \quad z = 0 . \tag{B.8}$$

Next, the total sound field in the half space $z > 0$ is written according to the perturbation procedure,

$$p(\vec{r}) = U_0(\vec{r}) + u(\vec{r}) , \tag{B.9}$$

where U_0 is the sound field for the flat mean surface and u is the first-order perturbation of the scattered field.

Substituting Eq. (B.9) in Eq. (B.8) and equating terms of the same order of Z^0 and Z, the boundary condition at $z = Z(x,y)$ becomes the boundary conditions at $z = 0$,

$$\begin{aligned} U_0(x,y) &= 0 , \\ u(x,y) &= -Z(x,y) \left| \frac{\partial U_0(\vec{r})}{\partial z} \right|_{z=0} . \end{aligned} \tag{B.10}$$

For an incident plane wave, the solution for a flat interface is given by

$$U_o(\vec{r}) = e^{i(\vec{k}_{i\perp}\cdot\vec{r}_\perp)}\left(e^{-ik_{iz}z} - e^{ik_{iz}z}\right). \tag{B.11}$$

From Eq. (B.10), the perturbation u at z = 0 is then

$$u(\vec{r}_\perp) = 2iZ(\vec{r}_\perp)k_{iz}e^{i\vec{k}_{i\perp}\cdot\vec{r}_\perp}. \tag{B.12}$$

Describing the surface waveheight $Z(\vec{r}_\perp)$ in Eq. (B.12) by a Fourier integral,

$$Z(\vec{r}_\perp) = \int_{-\infty}^{\infty} A(\vec{\kappa})\, e^{i\vec{\kappa}\cdot\vec{r}_\perp}\, d\vec{\kappa}, \tag{B.13}$$

where $\vec{\kappa}$ is the surface wave vector and $A(\vec{\kappa})$ is the complex amplitude of the constituent Fourier components, one can obtain a spectral representation for the perturbation field in the half-space z > 0,

$$u(\vec{r}_\perp) = 2ik_{iz}\int_{-\infty}^{\infty} A(\vec{\kappa})\, e^{i\left[(\vec{k}_{i\perp}+\vec{\kappa})\cdot\vec{r}_\perp + Zk_{sz}\right]}\, d\vec{\kappa}, \tag{B.14}$$

where $k_{sz} = \left[k_i^2 - (\vec{k}_{i\perp}+\vec{\kappa})^2\right]^{1/2}$ and $\mathrm{Im}(k_{sz}) > 0$.

Equation (B.14) implies that within the framework of the first-order perturbation theory, each Fourier component of the surface roughness gives rise to its own scattered plane wave in the direction $\vec{k}_s$ according to Bragg's law

$$\vec{k}_{s\perp} = \vec{k}_{i\perp} + \vec{\kappa}. \tag{B.15}$$

B22. Scattering Cross-section in the Far Field

From Eq. (B.14), the scattered sound intensity $I_s = \langle u\, u^* \rangle$ is written as

$$I_s = 4k_{iz}^2 \int_{-\infty}^{\infty}\!\!\int \langle A(\vec{\kappa})A^*(\vec{\kappa}')\rangle\, e^{i\left[(\vec{\kappa}-\vec{\kappa}')\cdot\vec{r}_\perp + (k_{sz}-k'_{sz})z\right]}\, d\vec{\kappa}\, d\vec{\kappa}', \tag{B.16}$$

where $k'_{sz} = \left[k_i^2 - (\vec{k}_{i\perp}+\vec{\kappa}')^2\right]^{1/2}$. The spectral amplitudes in the above equation are delta-correlated [A3], or

$$\langle A(\vec{\kappa})A^*(\vec{\kappa}')\rangle = S_s(\vec{\kappa})\,\delta(\vec{\kappa}-\vec{\kappa}'), \tag{B.17}$$

in which, as before, $S_s(\vec{K})$ is the spatial spectrum of the surface roughness.

Substitution of Eq. (B.17) into Eq. (B.16) yields

$$I_s = 4k_{iz}^2 \int_{-\infty}^{\infty} S_s(\vec{K})\, d\vec{K} . \tag{B.18}$$

In the far field zone, the scattered intensity can also be formally described by

$$I_s = \int_{\Sigma_{xy}} \sigma_{sc}(\theta_s, \varphi_s)\, r_s^{-2}\, d\Sigma_{xy} , \tag{B.19}$$

where $\sigma_{sc}(\theta_s, \varphi_s)$ is the scattering cross-section per unit solid angle per unit area for unit incident intensity, which is described here as a function of incident angle θ_s and azimuthal angle φ_s of the scattering direction and is integrated over the flat insonified area Σ_{xy}. It was demonstrated by Brekhovskikh [A3] that $d\Sigma_{xy} = r_s^2 \tan\theta_s\, d\theta_s\, d\varphi_s$ in the far-field approximation and $d\vec{K} = k_{sz}^2 \sin^2\theta_s \cos\theta_s\, d\theta_s\, d\varphi_s$. These results are inserted into Eqs. (B.18) and (B.19), which are then equated to result in

$$\int_0^{2\pi}\int_0^{\pi/2} \sigma_{sc}(\theta_s, \varphi_s) \tan\theta_s\, d\theta_s\, d\varphi_s = 4k_{iz}^2 \int_0^{2\pi}\int_0^{\pi/2} k_{sz}^2 S_s(\vec{K}) \sin\theta_s \cos\theta_s\, d\theta_s\, d\varphi_s , \tag{B.20}$$

or

$$\sigma_{sc}(\vec{k}_s) = 4k_{iz}^2 k_{sz}^2 S_s(\vec{K}) , \tag{B.21}$$

in which $\vec{k}_s$ and $\vec{k}_i$ are related by

$$\begin{aligned} k_{sy} &= k_{iy} , \text{ and} \\ \vec{K} &= \vec{k}_{s\perp} - \vec{k}_{i\perp} . \end{aligned} \tag{B.22}$$

In summary, Eq. (B.21) describes the coherent scattering cross-section for a static randomly rough ocean surface, which is seen from Eq. (B.22) to follow the familiar Bragg's law of scattering up to the first order of perturbation.

B23. Far Field Scattering Cross-section for a Moving Ocean Surface

So far the temporal variation of the ocean surface has not been included in the analysis of the scattered field. For this purpose, the moving surface displacement should be represented as a superposition of progressive surface waves,

$$\zeta(\vec{r}_\perp, t) = \mathrm{Re}\left\{ \int_{-\infty}^{\infty} A_0(\vec{K})\, e^{i(\vec{K}\cdot\vec{r}_\perp - \Omega t)}\, d\vec{K} \right\} , \tag{B.23}$$

where $\Omega = \Omega(K)$ is the frequency of the surface wave and $A_0(\vec{K})$ is its real amplitude. This amplitude is related to the spatial spectrum of the surface waves $S_0(\vec{K})$ by the following relationships

$$\begin{aligned} &\langle A_0(\pm\vec{K}) A_0^*(\pm\vec{K}') \rangle = 2S_0(\pm\vec{K})\delta(\vec{K}-\vec{K}'), \\ &\langle A_0(\pm\vec{K}) A_0^*(\mp\vec{K}') \rangle = 0 . \end{aligned} \tag{B.24}$$

Note that $S_0(\vec{K})$ is not the spatial spectrum of the motionless sea surface $S_S(\vec{K})$ and is related to the latter by

$$S_s(\vec{K}) = \frac{1}{2}\left[S_0(\vec{K}) + S_0(-\vec{K})\right] . \tag{B.25}$$

As for Eq. (B.14), the perturbation scattered field $u(\vec{r}_s,t)$ can be obtained in a similar manner, adding the time-dependent factors,

$$\begin{aligned} u(\vec{r}_s,t) = {} & ik_{iz}\int_{-\infty}^{\infty} A_0(\vec{K})\, e^{i\left[(\vec{k}_{i\perp}+\vec{K})\cdot\vec{r}_\perp + z k_{sz}^{(+)} - (\omega_0+\Omega)t\right]} d\vec{K} \\ & + ik_{iz}\int_{-\infty}^{\infty} A_0(\vec{K})\, e^{i\left[(\vec{k}_{i\perp}-\vec{K})\cdot\vec{r}_\perp + z k_{sz}^{(-)} - (\omega_0-\Omega)t\right]} d\vec{K} , \end{aligned} \tag{B.26}$$

where, with c being the sound velocity in water,

$$k_{sz}^{(\pm)} = \left[\left(\frac{\omega_0 \pm \Omega}{c}\right)^2 - \left(\vec{k}_{i\perp} \pm \vec{K}\right)^2\right]^{1/2} , \quad \mathrm{Im}\left(k_{sz}^{(\pm)}\right) > 0 . \tag{B.27a}$$

Applying the narrow-band approximation, $\Omega \ll \omega_0$, one rewrites $k_{sz}^{(\pm)}$ as

$$k_{sz}^{(\pm)} \simeq \left[k_i^2 - \left(\vec{k}_{i\perp} \pm \vec{K}\right)^2\right]^{1/2} . \tag{B.27b}$$

As $\vec{K}$ is replaced by $-\vec{K}$ in the second integral of Eq. (B.26), the scattered perturbation field now becomes

$$\begin{aligned} u(\vec{r}_s,t) = {} & ik_{iz}\int_{-\infty}^{\infty} \left[A_0(\vec{K})\, e^{-i(\omega_0+\Omega)t} + A_0(-\vec{K})\, e^{-i(\omega_0-\Omega)t}\right] \\ & e^{i\left[(\vec{k}_{i\perp}+\vec{K})\cdot\vec{r}_\perp + z k_{sz}\right]} d\vec{K} , \end{aligned} \tag{B.28}$$

where $k_{sz} = k_{sz}^{(+)}$. From Eq. (B.28), the temporal correlation function of the scattered field, $\Psi(\tau) = \langle u(\vec{r}_s,t)\, u^*(\vec{r}_s,t+\tau)\rangle$, is obtained through the use of relationships given in Eq. (B.24),

$$\Psi(\tau) = 2k_{iz}^2 \int_{-\infty}^{\infty} \left[S_0(\vec{K})\, e^{i(\omega_0+\Omega)\tau} + S_0(-\vec{K})\, e^{i(\omega_0-\Omega)\tau}\right] d\vec{K} . \tag{B.29}$$

In consideration of the far field zone and a finite scattering surface, Eq. (B.29) leads to

$$\sigma_{sc}(\vec{K},\omega) = 2k_{iz}^2 k_{sz}^2 \left[S_0(\vec{K})\,\delta(\omega-\omega_0-\Omega) + S_0(-\vec{K})\,\delta(\omega-\omega_0+\Omega)\right] , \tag{B.30}$$

following the steps similar to those taken from Eq. (B.18) to Eq. (B.21). Equation (B.30) describes two spectral lines shifted relative to ω_o by the value $\pm\Omega(K)$. Through the relationship presented in Eq. (B.25), the resulting scattering cross-section for a moving surface is reducible to that for a frozen surface after an integration of Eq. (B.30) over ω is performed.

B3. Kuperman

From the fundamental concepts initiated by Brekhovskikh [A3] and Bass and Fuks [A4], Kuperman carried out a more systematic analysis of the scattering problem from a general two-fluid interface using the perturbation method. However, his detailed treatment was mainly focused on scattering in the specular direction. In the following, we will summarize the major results contributed by Kuperman regarding scattering from the ocean surface.

B31. Generalized Boundary Conditions Transformed by the Perturbation Method

The geometry of a general two-fluid interface was considered with subscript 1 referring to the incident half-space and subscript 2 to the other half-space. Let U_i be the velocity potentials in the two half-spaces, the conditions that velocity and pressure be continuous across the interface could be stated as

$$\rho_1 U_1(\vec{r}) = \rho_2 U_2(\vec{r}) \quad \text{and} \quad \frac{\partial U_1(\vec{r})}{\partial \hat{n}} = \frac{\partial U_2(\vec{r})}{\partial \hat{n}} \tag{B.31}$$

at $z = Z(\vec{r}_\perp)$. These conditions were expanded in a Taylor series about $z = 0$ up to terms of the orders Z^2 and $\nabla_\perp Z$ [C8],

$$\rho_1 U_1(\vec{r}_\perp) + \rho_1 Z \left.\frac{\partial U_1}{\partial z}\right|_{z=0} + \rho_2 \frac{Z^2}{2} \left.\frac{\partial^2 U_1}{\partial z^2}\right|_{z=0} \tag{B.32}$$
$$= \rho_2 U_2(\vec{r}_\perp) + \rho_2 Z \left.\frac{\partial U_2}{\partial z}\right|_{z=0} + \rho_2 \frac{Z^2}{2} \left.\frac{\partial^2 U_2}{\partial z^2}\right|_{z=0},$$

$$\left.\frac{\partial U_1}{\partial z}\right|_{z=0} + Z \left.\frac{\partial^2 U_1}{\partial z^2}\right|_{z=0} + \frac{Z^2}{2} \left.\frac{\partial^3 U_1}{\partial z^3}\right|_{z=0} - (\nabla_\perp Z)\cdot(\nabla_\perp U_1) \tag{B.33}$$
$$= \left.\frac{\partial U_2}{\partial z}\right|_{z=0} + Z \left.\frac{\partial^2 U_2}{\partial z^2}\right|_{z=0} + \frac{Z^2}{2} \left.\frac{\partial^3 U_2}{\partial z^3}\right|_{z=0} - (\nabla_\perp Z)\cdot(\nabla_\perp U_2),$$

where one has used

$$\frac{\partial}{\partial \hat{n}} \approx \frac{\partial}{\partial z} - (\nabla_\perp Z)\cdot\nabla_\perp . \tag{B.34}$$

The velocity potential U_i was decomposed into the mean field $\langle U_i \rangle$ and the stochastic field u_i,

$$U_i = \langle U_i \rangle + u_i \quad , \quad i = 1,2 \; . \tag{B.35}$$

Substituting Eq. (B.35) into Eqs. (B.32) and (B.33), carrying out the averaging operation, and a simple algebraic manipulation lead to two separate sets of transformed boundary conditions on the plane z = 0 for the mean and perturbation fields:

(i) For $\langle U_i \rangle$ up to the Z^2 order,

$$\rho_1 \langle U_1 \rangle - \rho_2 \langle U_2 \rangle = F_1 \left(\langle U_1 \rangle, \langle U_2 \rangle, u_1, u_2 \right) \; , \tag{B.36a}$$

$$\frac{\partial \langle U_1 \rangle}{\partial z} - \frac{\partial \langle U_2 \rangle}{\partial z} = F_2 \left(\langle U_1 \rangle, \langle U_2 \rangle, u_1, u_2 \right) \; , \text{ and} \tag{B.36b}$$

(ii) For u_i up to the Z order,

$$\rho_1 u_1 - \rho_2 u_2 = G_1 \left(\langle U_1 \rangle, \langle U_2 \rangle \right) \; , \tag{B.37a}$$

$$\frac{\partial u_1}{\partial z} - \frac{\partial u_2}{\partial z} = G_2 \left(\langle U_1 \rangle, \langle U_2 \rangle \right) \; . \tag{B.37b}$$

Detailed expressions for F_1, F_2, G_1, and G_2 are given in Reference [C8]. In general, the method of solution suggested by Kuperman was to solve for the perturbation fields from Eq. (B.37) by the Fourier transform technique or spectral analysis and then to obtain the mean fields at the surface from Eq. (B.36). A critical step employed by Kuperman in obtaining a formal solution for the mean fields was to replace the mean fields in Eq. (B.36) by solutions to the flat-interface scattering problem. On one hand, this greatly reduced the algebraic complexity but, on the other hand, limited the accuracy of the resulting mean fields only to a lower order Z, instead of Z^2 as implied in the derivation procedure leading to Eq. (B.36).

B32. Reflection Coefficient for Scattering from the Ocean Surface

For the pressure-release case, the boundary conditions represented by Eqs. (B.36a) and (B.37a) reduce to

$$\left| \langle U \rangle \right|_{z=0} = - \left| \langle z \frac{\partial u}{\partial z} \rangle \right|_{z=0} \; , \tag{B.38}$$

$$\left| u \right|_{z=0} = - z \left| \frac{\partial \langle U \rangle}{\partial z} \right|_{z=0} \; , \tag{B.39}$$

in which the unsubscripted fields refer to scattered fields in medium 1. Following the procedure briefly described above, Kuperman derived the expression for the mean field at the surface

$$\langle U \rangle = 2k_{iz} e^{i\vec{k}_{i\perp}\cdot\vec{r}_\perp} \int_{-\infty}^{\infty} k_{sz} S_s(\vec{K})\, d\vec{K} , \tag{B.40}$$

which has been translated into our present terminology from Eq. (61) of Reference [C8]. Note that the spatial spectrum of the surface roughness defined by Kuperman differs from $S_s(K)$ by a factor 2π. When the mean field is cast in the form of a flat-interface solution

$$U_o(\vec{r}_s) = e^{i\vec{k}_{i\perp}\cdot\vec{r}_\perp} \left(e^{-izk_{iz}} + R e^{izk_{iz}} \right) , \tag{B.41}$$

with R being the specular reflection coefficient, then R can be identified from Eq. (B.40) as

$$R = -1 + 2k_{iz} \int_{-\infty}^{\infty} k_{sz} S_s(\vec{K})\, d\vec{K} , \tag{B.42}$$

where k_{sz} has been determined from Eq. (B.27b).

At this point, it is interesting point out that Brekhovskikh [A3, Section 9.6] arrived at the same result by employing a rather heuristic approach. On the basis of energy conservation, Brekhovskikh reasoned that "the vertical energy flux through a unit surface in the incident wave had to be equal to the sum of the flux in the reflected and scattered waves." From Eq. (B.18), this was translated into the following mathematical statement

$$\cos\theta_i = |R|^2 \cos\theta_i + 4k_{iz}^2 \int_{-\infty}^{\infty} \cos\theta_s S_s(\vec{K})\, d\vec{K} , \tag{B.43}$$

where θ_i and θ_s are the incident and scattering angles, respectively. Equation (B.43) was rewritten as

$$|R|^2 = 1 - 4k_i \cos\theta_i \int_{-\infty}^{\infty} k_{sz} S_s(\vec{K})\, d\vec{K} , \tag{B.44}$$

in which $\cos\theta_s$ has been replaced by

$$\cos\theta_s = \frac{k_{sz}}{k_i} . \tag{B.45}$$

Under the approximation that the scattering contribution represented by the integral in Eq. (B.44) is much smaller than unity, Brekhovskikh described the reflection coefficient as

$$|R| = 1 - 2k_{iz} \int_{-\infty}^{\infty} k_{sz} S_s(\vec{K})\, d\vec{K}\,, \tag{B.46}$$

which is equivalent to Eq. (B.42).

An approximate expression for $|R|$ was also obtained by Brekhovskikh under the assumption that the spatial spectrum $S_s(\vec{K})$ is not significant when $K > 1/\Lambda_0$, with Λ_0 being the correlation length of the rough surface. First, the radical factor in the integrand in Eq. (B.46) was rewritten as

$$\begin{aligned} k_{sz} &= \left[k_i^2 - (\vec{k}_{i\perp} + \vec{K})^2\right]^{1/2} \\ &= k_i \left[\cos\theta_i - 2\frac{K}{k_i}\sin\theta_i \cos(\alpha - \varphi_i) - \frac{K^2}{k_i^2}\right]^{1/2}, \end{aligned} \tag{B.47}$$

where (θ_i, φ_i) described the direction of the incident wave and $\vec{K} = (K\cos\alpha, K\sin\alpha)$. The above assumption implies that $k\Lambda_0 \cos^2\theta_i \gg 1$, thus simplifying Eq. (B.47),

$$\left[k_i^2 - (\vec{k}_{i\perp} + \vec{K})^2\right]^{1/2} \simeq k_i \cos\theta_i = k_{iz}\,. \tag{B.48}$$

Hence the reflection coefficient of Eq. (B.46) became

$$|R| \simeq 1 - 2k_{iz}^2 \int_0^{\infty} \int_{-\pi}^{\pi} S_s(K, \alpha)\, K\, dK\, d\alpha \tag{B.49}$$

or

$$|R| \simeq 1 - 2\sigma^2 k_{iz}^2\,, \tag{B.50}$$

where $\sigma^2 = \langle z^2 \rangle$.

B33. Scattering Kernel and Reflection Coefficient for a Moving Ocean Surface

In addition to the above analyses for a frozen rough surface, Kuperman also investigated [C6] the case of a dynamic ocean surface. In this extended case, he generalized the expression described by Eq. (B.42) for the reflection coefficient and also derived the scattering kernel for the nonspecular direction. In deriving the scattering kernel, Kuperman employed a spectral analysis approach with the narrow-band approximation essentially similar to

Brekhovskikh's treatment presented earlier, except that he focused on the scattering kernel but not on a far-field scattering cross-section like Brekhovskikh. Because of this, his scattering kernel is equivalent, except for a z-dependent factor, to that implied by Eq. (B.30), which was derived by Brekhovskikh for the far-field case. This scattering kernel in our present notation is of the form (see Eq. (8a) of Reference [C8]),

$$M(\vec{K},\omega) = 2k_{iz}^2 \left[e^{-\Delta^{(+)}z} S_0(\vec{K})\,\delta(\omega-\omega_0-\Omega) + e^{-\Delta^{(-)}z} S_0(-\vec{K})\,\delta(\omega-\omega_0+\Omega) \right], \tag{B.51}$$

where

$$\Delta^{(\pm)} = \begin{cases} 2\left|k_{sz}^{(\pm)}\right| & \text{if } k_{sz}^{(\pm)} \text{ is real,} \\ 0 & \text{if } k_{sz}^{\pm} \text{ is complex,} \end{cases} \tag{B.52}$$

with $k_{sz}^{(\pm)}$ given by Eq. (B.27a). Note that in the limit $z \to \infty$, the scattering kernel presented in Eq. (B.51) is identical to the scattering kernel derivable from Eq. (B.30).

Inclusion of the temporal variation also enabled Kuperman to modify his expression (Eq. (B.42)) for the reflection coefficient to decompose the reflected field in two Doppler-shifted components. Starting from the boundary conditions represented by Eqs. (B.38) and (B.39), using the spectral analysis approach, and replacing the mean fields with the flat-surface solutions, Kuperman derived the following reflection coefficient for a dynamic ocean surface [C6, Eq. (9c)]

$$R = -1 + k_{iz} \int \left(k_{sz}^{(+)} + k_{sz}^{(-)} \right) S_s(\vec{K})\, d\vec{K} . \tag{B.53}$$

APPENDIX C

Composite-Roughness Approach

In Appendices A and B, we have discussed two fundamental approaches to the theoretical solution of the problem of scattering from the ocean surface: the perturbation method and the tangent plane method. By their basic assumptions, the perturbation method tends to ignore the influence of the large-scale roughness while the tangent plane method could not reflect the contribution of the small-scale surface waves. A modification to the perturbation method was suggested to include scattering from the entire surface spectrum and was normally referred to as the composite-roughness approach. In the perturbation method, the randomly rough surface was conceived as a perturbation from the flat interface between the two media. By this principle, the perturbation method solution was constructed from two fundamental steps: first, the pressure release condition at the ocean surface was expanded about the flat interface with only terms of low orders being kept for consideration; and second, the scattered field was described by two components: the perturbation field and the unperturbed field, of which the latter was a solution to the flat-surface problem. In order to improve the perturbation method solution, the composite-roughness approach divides the ocean surface spectrum into two parts, high-frequency and low-frequency sections. The low-frequency part describes the spectral power of the large-scale roughness and the high-frequency part corresponds to the small-scale roughness. The perturbation procedure is then applied in a similar manner except that the flat interface as the unperturbed boundary is now replaced with the large-scale randomly rough surface. Several authors have employed this approach to investigate the surface scattering problem [D1-D3,A4]. In this chapter, we will summarize a heuristic formulation by Bachmann [D1] and a more rigorous treatment by McDaniel and Gorman [D3] for the backscattering case. We will also extend the results of McDaniel and Gorman to the general scattering case.

C1. Bachmann

Bachmann reasoned that the first-order perturbation theory was valid only for the small-scale rough surface $\mathcal{E}_S$. The large-scale rough surface $\mathcal{E}_L$ was then taken into account by modulation of the local grazing angle. On the basis of this heuristic conception, Bachmann set out to improve the result of the perturbation theory as follows. In fact, the following discussion is slightly more general than that presented in Reference [D1] by Bachman but essentially represents the same results. Figure C1 illustrates that, due to the presence of the large-scale roughness, the nominal grazing angle θ_i in the solution of the perturbation method should be replaced by the local grazing angle θ_ℓ, which deviates from θ_i by the local slope ϵ of the large-scale surface. Therefore, in the backscattering case, the scattering cross-section should be written as (see Eq.(B.21), for example)

$$\sigma_{sc}(\theta_\ell) = 4k_i^4 \sin^4\theta_\ell \, S_s(2k_i\cos\theta_i, 0) \,, \tag{C.1}$$

where S_ϵ is the two-dimensional spatial surface spectrum. The new backscattering cross-section is then determined by averaging $\sigma_{sc}(\theta_\ell)$ with respect to the local slope ϵ,

$$\langle \sigma_{sc}(\theta_\ell) \rangle_\epsilon = \langle \sigma_{sc}(\theta_i - \epsilon) \rangle_\epsilon \,. \tag{C.2}$$

Noting that $\sin^4\theta_\ell \simeq \theta_\ell^4$ as $\theta_\ell \to 0$, Bachmann used an approximation that allowed the averaging process to be operated over θ_ℓ instead of over $\sigma_{sc}(\theta_\ell)$. As a result, this is formally equivalent to attributing an inclination to the mean sea surface,

$$\langle \sigma_{sc}(\theta_i - \epsilon) \rangle_\epsilon = \sigma_{sc}(\theta_i + \Delta\theta) \,, \tag{C.3}$$

where $\Delta\theta$ is determined from the averaging operation,

$$\begin{aligned} (\theta_i + \Delta\theta)^4 &\simeq \langle (\theta_i - \epsilon)^4 \rangle_\epsilon \\ &= \theta_i^4 - 4\langle \epsilon \rangle \theta_i^3 + 6\langle \epsilon^2 \rangle \theta_i^2 - 4\langle \epsilon^3 \rangle \theta_i + \langle \epsilon^4 \rangle \,. \end{aligned} \tag{C.4}$$

Under the assumption that the local surface slope is normally distributed and its mean value is zero, the expectation values of all odd moments vanish and those of even moments are given by

$$\langle \epsilon^{2n} \rangle = (2n-1)!!\, \epsilon_{rms}^{2n} \,, \tag{C.5}$$

where ϵ_{rms} is the rms value of ϵ. Thus, according to this heuristic composite-roughness approach, the backscattering cross-section is described by

$$\sigma_{sc}(\theta_i) = 4k_i^4 \sin^4(\theta_i + \Delta\theta)\, S_s(2k_i \cos\theta_i, 0) \,, \tag{C.6}$$

in which $\Delta\theta$ is specified by

$$\Delta\theta = \left(\theta_i^4 + 6\theta_i^2 \epsilon_{rms}^2 + 3\epsilon_{rms}^4 \right)^{1/4} - \theta_i \,. \tag{C.7}$$

C.2 McDaniel and Gorman

In the preceding section was presented an ad-hoc modification to the backscattering solution of the perturbation theory employing the composite-roughness concept. On the basis of the same physical picture, McDaniel and Gorman [D3], however, rigorously applied a perturbation procedure to the backscattering case. They followed the perturbation procedure initiated by

Labianca and Harper [C1-C5] but considered the large-scale rough surface as the unperturbed surface instead of the flat interface. McDaniel and Gorman started from a Green's function form of the solution to the Helmhotz equation

$$U(\vec{r}_2,\vec{r}_s) = G_0(\vec{r}_2,\vec{r}_s) - \frac{1}{4\pi}\int_{\mathcal{L}_L}\left[G_0(\vec{r},\vec{r}_2)\hat{n}\cdot\nabla U(\vec{r},\vec{r}_s) - U(\vec{r},\vec{r}_s)\hat{n}\cdot\nabla G_0(\vec{r},\vec{r}_2)\right]_{\mathcal{L}_L} d\mathcal{L}_L , \tag{C.8}$$

where $U(\vec{r}_2,\vec{r}_s)$ is the total scattered field, $G_0(\vec{r}_2,\vec{r}_s)$ is the Green function to be chosen appropriately with the boundary conditions, $\hat{n}$ is the unit vector normal to the large-scale surface, and the integration is to be carried over the large-scale surface $\mathcal{L}_L$. The scattered field is next expressed as a series in the small parameter σ, the rms waveheight of the small-scale surface $\mathcal{L}_S$, up to the second order

$$U(\vec{r}_2,\vec{r}_s) = U_0(\vec{r}_2,\vec{r}_s) + \sigma U_1(\vec{r}_2,\vec{r}_s) + \sigma^2 U_2(\vec{r}_2,\vec{r}_s) . \tag{C.9}$$

Since the integration in Eq.(C.8) is over $\mathcal{L}_L$, the pressure-release boundary condition at $\mathcal{L}_S$ needs to be transformed to $\mathcal{L}_L$. This can be achieved by first expanding $[U]_{\mathcal{L}_S}$ about $\mathcal{L}_L$ as

$$[U]_{\mathcal{L}_S} = \left[U + z_\perp \hat{n}\cdot\nabla U + \frac{z_\perp^2}{2}(\hat{n}\cdot\nabla)^2 U\right]_{\mathcal{L}_L} , \tag{C.10}$$

where $z_\perp$ is the waveheight of $\mathcal{L}_S$ with respect to $\mathcal{L}_L$. Applying the boundary condition $[U]_{\mathcal{L}_S} = 0$, using Eq.(C.9), and equating terms of the same powers of σ yield

$$[U_0]_{\mathcal{L}_L} = 0 , \tag{C.11a}$$

$$[U_1]_{\mathcal{L}_L} = -\left[z_\perp \hat{n}\cdot\nabla U_0\right]_{\mathcal{L}_L} , \text{ and} \tag{C.11b}$$

$$[U_2]_{\mathcal{L}_L} = -\left[z_\perp \hat{n}\cdot\nabla U_1\right]_{\mathcal{L}_L} - \left[\frac{z_\perp^2}{2}(\hat{n}\cdot\nabla)^2 U_0\right]_{\mathcal{L}_L} . \tag{C.11c}$$

Substituting Eqs.(C.9) and (C.11) into Eq.(C.8) and equating terms of the same powers of σ lead to

$$U_0(\vec{r}_2,\vec{r}_s) = G_0(\vec{r}_2,\vec{r}_s) - \frac{1}{4\pi}\int_{\mathcal{L}_L}\left[G_0(\vec{r},\vec{r}_2)\hat{n}\cdot\nabla U_0(\vec{r},\vec{r}_s)\right]_{\mathcal{L}_L} d\mathcal{L}_L , \tag{C.12a}$$

$$\sigma U_1(\vec{r}_2,\vec{r}_s) = -\frac{\sigma}{4\pi}\int_{\mathcal{L}_L}\left[G_0(\vec{r},\vec{r}_2)\hat{n}\cdot\nabla U_1(\vec{r},\vec{r}_s)\right]_{\mathcal{L}_L} d\mathcal{L}_L - \frac{1}{4\pi}\int_{\mathcal{L}_L}\left[z_\perp \hat{n}\cdot\nabla U_0(\vec{r},\vec{r}_s)\hat{n}\cdot\nabla G_0(\vec{r},\vec{r}_2)\right]_{\mathcal{L}_L} d\mathcal{L}_L , \tag{C.12b}$$

$$\sigma^2 U_2(\vec{r}_2,\vec{r}_s) = -\frac{\sigma^2}{4\pi}\int_{\mathcal{L}_L}\left[G_0(\vec{r},\vec{r}_2)\hat{n}\cdot\nabla U_2(\vec{r},\vec{r}_s)\right]_{\mathcal{L}_L} d\mathcal{L}_L - \frac{1}{4\pi}\int_{\mathcal{L}_L}\left\{\left[\sigma z_\perp \hat{n}\cdot\nabla U_1(\vec{r},\vec{r}_s) + \frac{z_\perp^2}{2}(\hat{n}\cdot\nabla)^2 U_0(\vec{r},\vec{r}_s)\right]\hat{n}\cdot\nabla G_0(\vec{r},\vec{r}_2)\right\}_{\mathcal{L}_L} d\mathcal{L}_L . \tag{C.12c}$$

The above set of integral equations define the formal solution of the scattered field up to the second perturbation order. Since results obtained by the perturbation method indicated that information on the scattered field was contained in the first and higher-order perturbation components, McDaniel and Gorman proceeded to solve for U_1 by taking two key steps: (i) The Green's function was chosen to be the Green's function for the problem of scattering from the large-scale surface alone, that is G_0 vanishes on Σ_L; and (ii) The Kirchhoff's approximation was assumed for the unperturbed component. From Eqs.(C.11a) and (C.12a), the first step implies

$$U_0(\vec{r}_i, \vec{r}_s) = G_0(\vec{r}_i, \vec{r}_s) \text{ and } [U_0]_{\Sigma_L} = [G_0]_{\Sigma_L} = 0 \ . \tag{C.13}$$

In addition, the Kirchhoff's assumption on U_0 leads to

$$[\hat{n} \cdot \nabla U_0]_{\Sigma_L} = -[2\hat{n} \cdot \nabla U_{inc}]_{\Sigma_L} \ , \tag{C.14}$$

where U_{inc} is the incident acoustic field.

For a point source and a receiver located in the far field, one can write

$$U_{inc}(\vec{r}, \vec{r}_i) = \frac{\exp[i\vec{k}_i \cdot (\vec{r}_i + \vec{r})]}{|\vec{r}_i|} \tag{C.15}$$

and obtain

$$[\hat{n} \cdot \nabla U_0]_{\Sigma_L} = 2i\hat{n} \cdot \vec{k}_i \ \frac{\exp[i\vec{k}_i \cdot (\vec{r}_i + \vec{r})]}{|\vec{r}_i|} \ . \tag{C.16}$$

Substitution of Eqs.(C.13) and (C.16) into Eq.(C.12b) yields

$$\nabla U_1(\vec{r}_i, \vec{r}_s) = -\frac{1}{\pi} \int_{\Sigma_L} \frac{\hat{n} \cdot \vec{k}_i}{|\vec{r}_i|} \ \frac{\hat{n} \cdot \vec{k}_s}{|\vec{r}_s|} \exp\left\{i\left[\vec{k}_i \cdot \vec{r}_i + \vec{k}_s \cdot \vec{r}_s - (\vec{k}_s \cdot \vec{k}_i) \cdot \vec{r}\right]\right\} d\Sigma_L \ . \tag{C.17}$$

From the scattered field described by the above equation, McDaniel and Gorman performed the ensemble averaging operation over the large-scale surface to obtain the scattered intensity

$$I_s = \frac{2A}{r_i^2 r_s^2} \langle (\hat{n} \cdot \vec{k}_i)^2 (\hat{n} \cdot \vec{k}_s)^2 \rangle_{\Sigma_L} \left[S_0(\vec{K}) + S_0(-\vec{K})\right] \ , \tag{C.18}$$

where A is the insonified area and

$$\vec{K} = \vec{k}_{sL} - \vec{k}_{iL} \ . \tag{C.19}$$

From Eq. (C.18) the general scattering cross-section is given by

$$\sigma_{sc} = 2\left\langle (\hat{n}\cdot\vec{k}_i)^2 (\hat{n}\cdot\vec{k}_s)^2 \right\rangle_{\Sigma_L} \left[S_0(\vec{K}) + S_0(-\vec{K}) \right] , \tag{C.20}$$

which is reduced to the backscattering case as

$$\sigma_{sc} = 4\left\langle (\hat{n}\cdot\vec{k}_i)^4 \right\rangle_{\Sigma_L} S_s(2k_i\cos\theta_i, 0) , \tag{C.21}$$

which is identical to the earlier result (compare Eq. (C.1)) obtained by the heuristic formulation.

C.3 Two-dimensional Scattering Cross-Section

Above one has seen the derivation of the scattering cross-section by the composite-roughness approach in both heuristic and rigorous manners. But only for the backscattering case, this cross-section could be reduced to a practically useful form (see Eqs. (C.6) and (C.7)) through the use of an approximate averaging procedure suggested by Bachmann. In this section, we will employ a similar procedure to perform the averaging operation required in Eq. (C.20) for the case of two-dimensional scattering, or scattering in the plane of incidence. In this case, one can write the term that needs to be averaged in Eq. (C.20) as

$$\left\langle (\hat{n}\cdot\vec{k}_i)^2 (\hat{n}\cdot\vec{k}_s)^2 \right\rangle = k_i^4 \left\langle \sin^2\theta_i \sin^2\theta_s \right\rangle . \tag{C.22}$$

As in Section C.1, the scattering cross-section averaged over the local slope ϵ can be formally represented by

$$\left\langle \sigma_{sc}(\theta_i - \epsilon, \theta_s - \epsilon) \right\rangle_\epsilon = \sigma_{sc}(\theta_i + \Delta\theta, \theta_s + \Delta\theta) , \tag{C.23}$$

in which the average inclination $\Delta\theta$ is determined by the following averaging operation

$$(\theta_i + \Delta\theta)^2 (\theta_s + \Delta\theta)^2 = \left\langle (\theta_i - \epsilon)^2 (\theta_s - \epsilon)^2 \right\rangle . \tag{C.24}$$

Again, assuming the same statistical description for the local slope ϵ as in Section C.1, one can write Eq. (C.24) as

$$(\theta_i + \Delta\theta)^2 (\theta_s + \Delta\theta)^2 = \theta_i^2\theta_s^2 + \epsilon_{rms}^2 (\theta_i^2 + \theta_s^2 + 4\theta_i\theta_s) + 3\epsilon_{rms}^4 , \tag{C.25}$$

which can be solved for $\Delta\theta$,

$$\Delta\theta = -\frac{S_\theta}{2} + \frac{1}{2}\left\{S_\theta^2 - 4P_\theta + 4\left[P_\theta^2 + \epsilon_{rms}^2\left(S_\theta^2 + 2P_\theta\right) + 3\epsilon_{rms}^4\right]^{1/2}\right\}^{1/2}, \tag{C.26}$$

where

$$S_\theta = \theta_i + \theta_s \quad , \quad P_\theta = \theta_i \theta_s \ . \tag{C.27}$$

Notice that Eq. (C.26) is reducible to Eq. (C.7) when $\theta_s = \theta_i$. Therefore, the two-dimensional scattering cross-section is finally of the form

$$\sigma_{sc}(\theta_i, \theta_s) = 2k_i^4 \sin^2(\theta_i + \Delta\theta)\sin^2(\theta_s + \Delta\theta)\left[S_0(\vec{K}) + S_0(-\vec{K})\right] \tag{C.28}$$

with $\Delta\theta$ being given in Eq. (C.26).

APPENDIX D

Empirical Modeling

So far we have been concerned with descriptions of ocean surface scattering which are based on cohesive theoretical formulations. There exist, however, other descriptions of the surface scattering cross-section which essentially represent some forms of empirical fitting of data obtained in field measurements. In view of the considerably complex nature of the surface scattering problem and due to limited validity of most existing theories, these empirically-derived descriptions under appropriate conditions have proved to be rather useful. A major constraint in their use has to do with the fact that they are available only for the backscattering case. In this appendix, we will discuss two of the more established empirical models of surface backscattering that are mentioned most often in the literature.

D.1 Chapman-Harris

The Chapman-Harris [E4] empirical model of surface backscattering represents a best fit of measurements made in the early sixties for a range of wind speeds, grazing angles, and frequencies. In these data, backscattering strength is given in octave bands from 400 Hz to 6.4 KHz for 0-40° grazing angle and 0-30 knot wind speed. For most reported frequency bands and wind speeds, these backscattering data when plotted against grazing angle are characterized by two distinct features: first, in the range 10-40°, backscattering strength is strongly dependent on grazing angle; second, at lower grazing angles backscattering strength is relatively independent of grazing angle. Intuitively, Chapman and Harris attributed these two distinct scattering features to contributions from two different mechanisms, the first due to scattering from surface roughness and the second due to volume scattering from a layer of isotropic scatterers. Employing only those portions of the scattering strength versus grazing angle curves corresponding to roughness scattering, Chapman and Harris constructed an empirical formula of backscattering strength as a function of grazing angle, acoustic frequency, and wind speed. This formula was obtained in the form

$$\sigma_{CH} = 3.3\beta \log \frac{\theta_i}{30} - 42.4 \log \beta + 2.6 , \qquad (D.1)$$

in which

$$\beta = 158 \left(v f^{1/3}\right)^{-0.58} , \qquad (D.2)$$

where

σ_{CH} = backscattering strength in dB/μPa,
θ_i = grazing angle in degrees,
v = wind speed in knots, and
f = acoustic frequency in Hz.

Although the Chapman-Harris formula has been used extensively, attention must be drawn to the fact that its domain of validity should be constrained within 10-40° grazing angles, 0-30 knot wind speeds, and 400-6400 Hz frequencies.

D.2 Martin

Martin's approach [E1] to empirical modeling to the backscattering problem is slightly different to that of Chapman and Harris. Instead of direct fitting of experimental measurements, Martin constructed his model on the basis of several theoretical results and used available acoustic and optical reverberation data to estimate some key parameters built in these theoretical results. This observation will become clearer in the description of Martin's model below.

Martin perceived the surface scattering strength as being composed of three elements: roughness scattering (σ_S), sublayer bubble scattering (σ_B), and facet reflection and diffraction (σ_R). The total backscattering strength is then written as

$$\sigma_M = \sigma_S + \sigma_B + \sigma_R \,. \tag{D.3}$$

For the roughness scattering element, Martin used the backscattering cross-section derived by Kuo [C17] as an extension of Marsh's theory for the case of an impedance interface. This result is indeed reducible to that of Marsh or the first-order perturbation theory for the case of a pressure-release surface. In our notation, the roughness scattering component is then given as

$$\sigma_S = 4k_i^4 \sin^4\theta_i S_S(2k_i\cos\theta_i, 0) \,, \tag{D.4}$$

in which Martin suggested to deduce the two-dimensional surface spectrum from reverberation data if not otherwise available. Inferring from the available data, Martin also proposed to modify the use of the above expression near normal incidence. Specifically, he suggested

$$\sigma_S(\theta_i \geq 60°) = \sigma_S(\theta_i = 60°) \,. \tag{D.5}$$

With regard to the second element of bubble scattering, Martin applied the general theory of volume scattering developed by Tatarski [V. I. Tatarski, "Wave propagation in a turbulent medium," McGraw-Hill, New York, 81-90 (1961)] to scattering by sublayer bubbles. The general result of Tatarski was derived

for an isotropic distribution of volume scatterers such as, for example, temperature fluctuation, salinity fluctuation, or subsurface bubbles. The backscattering strength for these types of scatterers is of the form

$$\sigma_B = 2\pi k_i^4 \sin\theta_i \left\{ z_0(k_i) \frac{S_x^{(3)}(2k_i)}{x^2} \right\}, \tag{D.6}$$

where, in the case of bubbles,

x = characteristic length of bubbles,
z_0 = effective depth at which scattering of k_i takes place, and
$S_x^{(3)}$ = three-dimensional power spectrum of x.

In absence of actual data, the biased power spectrum, which is the term contained in the curly brackets in Eq. (D.6), was estimated by Martin from the acoustic reverberation data. This results in

$$z_0(k_i) \frac{S_x^{(3)}(2k_i)}{x^2} = B v^{2.91} k_i^{-3.143}, \tag{D.7}$$

in which

B = 1.25×10^{-6}, a fitting constant,
v = wind speed in knots, and
k_i = incident wave number in cm^{-1}.

Martin also proposed to modify the use of the above fitting formula, Eq. (D.7), as dictated by the involved data such that

$$\begin{aligned} \sigma_B(v \le 5 \text{ knots}) &= \sigma_B(v = 5 \text{ knots}), \\ \sigma_B(v \ge 15 \text{ knots}) &= \sigma_B(v = 15 \text{ knots}), \end{aligned} \tag{D.8}$$

and to restrict its application to

$$0.05 \le 2k_i \le 5 \text{ cm}^{-1} \quad \text{or} \quad 0.6 \le f \le 60 \text{ KHz}. \tag{D.9}$$

Finally, the contribution by facet reflection/diffraction, based on his own analysis [E2], was modeled as

$$\sigma_R = \sigma_{R0} \exp\left[-\frac{1}{2} \left(\frac{\cot\theta_i}{\sigma'} \right)^2 \right], \tag{D.10}$$

in which

$$\sigma_{R0} = \frac{1}{\pi} \left(\frac{\sigma''^2}{\sigma' \sigma'''} \right)^2, \tag{D.11}$$

where σ', σ'', and σ''' are the variances of the first, second, and third derivatives of the surface elevation. Since these statistics are often not available, Martin proposed to estimate σ' and σ_{R0} from the acoustic and optic data of surface wave spectra. The results are

$$\sigma'^2 = \frac{1}{2}\left(0.003 + 0.00264\, v\right) \tag{D.12}$$

and for σ_R at normal incidence

$$\sigma_{R0} = \begin{cases} 10 - 10 \log v^{1.68}, & 2 \le v \le 20 \text{ knots} \\ -13 \text{ dB}, & v > 20 \text{ knots}. \end{cases} \tag{D.13}$$

where the wind speed v is in knots.

In summary, one notes that Martin's model is a synthesis of theoretical analyses available at the time, which are then correlated to acoustic and optic data on acoustic reverberation and surface wave spectra to estimate the involved environmental parameters. The final output is an analytical-empirical description of the backscattering strength as a function of grazing angle, wind speed, and frequency. The physical rationale to construct such a model is driven primarily by the cognition that acoustic scattering from the sea surface is dominated by three mechanisms in three overlapping ranges of grazing angles: bubble scattering (0°-50°), roughness scattering (30°-70°), and facet reflection (70°-90°).

APPENDIX E

Empirical Modeling of Surface Wave Spectra

The spectrum of ocean surface waves is the most critical input that determines the performance of any scattering theory. Since the processes governing generation and development of ocean waves are very complex, a cohesive theory that is expected to provide an adequate description of these surface waves, including the resultant wave spectra, until now has been unavailable. Consequently, most computations that require spectra as input have made use of descriptions empirically derived. These empirical relationships should be used with care due to lack of universal agreement and considerable errors associated with many of the measurement techniques.

Of all the various types of wave motion in the ocean, we will be only concerned with those surface waves which are generated by the interaction of the wind with the ocean surface. An important distinction should be made here between "gravity" and "capillary" waves. Surface gravity waves are caused by the wind and propagate under the restoring force of gravity. Their wavelengths range from about 10 cm to about 1 km, with maximum energy density typically centered about the wavelength of 150 m. Popular names for gravity waves include "sea waves" for rough irregular waves near a storm area, and "swells" for smooth almost-sinusoidal waves at some distance from the storm center. On the other hand, capillary waves are also generated by the wind but propagate under the restoring force of surface tension. They are sometimes referred to as "ripples" with wavelengths less than about 1 cm and their amplitude considerably less than that of gravity waves. Caution should be taken to differentiate between these two types of surface waves because they are characterized by two different dispersion relationships. In this study, the term "ocean surface waves" are used to denote both types and the following combined dispersion relationship is valid for the entire range of wavelengths,

$$\omega^2 = gk\left(1 + \frac{k^2}{k_m^2}\right), \tag{E.1}$$

where

$$k_m = \left(\frac{g\rho}{\tau}\right)^{\frac{1}{2}},$$

in which

ω = angular frequency,
k = wave number,
g = gravitational acceleration,
ρ = water density, and
τ = surface tension.

The first serious attempt to model the one-dimensional spectrum was probably made by Phillips [K14] for those frequencies that are higher than that of the peak in the observed spectrum and lower than frequencies for which surface tension is important. This range of frequencies is known as the "equilibrium range", in which the stability of the water surface is maintained, i.e., when the surface waves have reached equilibrium under the given wind conditions in the sense that they cannot grow any higher without breaking. On the basis of dimensional analysis, Phillips derived that the one-dimensional energy spectrum decreased with increasing frequency (f) as the inverse fifth power of the frequency, or

$$S_p(f) = \mu g^2 f^{-5}, \tag{E.2}$$

where μ = 18.3 x 10^{-4} (MKS), Phillips' dimensionless equilibrium range constant.

In the absence of measurements of surface wave energy as a function of fetch, wind duration and water depth, the modeling efforts continued to be developed for idealized conditions. One of such considerations indeed led to the fairly popular and useful concept of a "fully-developed spectrum". The physical idea is as follows. In an ocean initially at rest, a steady wind commences to blow over an infinite surface. Waves of high frequency will grow fast and reach equilibrium quickly. Waves of successively lower and lower frequency will then grow to equilibrium, filling Phillips' equilibrium range. The waves of very low frequency will grow to a certain extent until their phase velocity becomes faster than the wind speed. One expects then both low and high cutoffs in frequencies with a peak at about the frequency for which the wave phase speed equals the wind speed. Therefore, after a sufficiently long duration, one anticipates that the entire spectrum will reach a steady state and will be fully developed. Although, it appears limited, this conceptualized spectrum has proved to be rather useful for description of surface waves in the open ocean. Pierson and Moskowitz [K10,K11] proposed the following fully-developed spectrum model to fit their observed data,

$$S_{PM}(\omega) = \alpha \frac{g^2}{\omega^5} e^{-\beta (\omega_0/\omega)^4}, \tag{E.3}$$

where

ω_0 = g/u,
α = 0.0081 (MKS),
β = 0.74 (MKS), and
u = wind speed (m/s).

This spectrum model was extensively used in many calculations and was continually updated with new measurements for various frequency ranges [K3,K5, K7,K9]. The latest version developed by Pierson [K4] represents a systematic synthesis of several data sources to cover the broadest possible frequency

range. It is this version that will be used in the present study. In general, Pierson organizes the one-dimensional fully-developed spectrum into six ranges, each of which is described by two sets of expressions. One set is to express the spectrum in terms of frequency and the other in terms of wave number. They are related to one another through a specific dispersion relationship, which is dictated by the dominant generation mechanism, either gravity or capillary, for that particular frequency range. This model is summarized as follows:

A. Pierson-Moskowitz Range

Frequency: $[0, \omega_A]$
Wave Number: $[0, k_A]$
Dispersion Relationship: $\omega^2 = kg$ (gravity)
Empirical Formulae:

$$S_A(\omega) = \alpha \frac{g^2}{\omega^5} e^{-\beta(\omega_0/\omega)^4} \tag{E.4}$$

$$S_A(k) = \frac{\alpha}{2k^3} e^{-\beta(k_0/k)^2} \tag{E.5}$$

Parameters:

$\omega_0 = g/u$
$\omega_A = (4\beta/5)^{1/4}\omega_0$
$k_0 = g/u^2$
$k_A = (2/3)^{1/2} k_0$
$\alpha = 0.0081$ MKS
$\beta = 0.74$ MKS

B. Stacy Range

Frequency: $[\omega_A, \omega_B]$
Wave Number: $[k_A, k_B]$
Dispersion Relationship: $\omega^2 = gk$ (gravity)
Empirical Formulae:

$$S_B(\omega) = \begin{cases} S_A(\omega) & \text{for } u_* < u_{*B} \\ \text{Max}\left[S_A(\omega), S_B^*(\omega)\right] & \text{for } u_* \geq u_{*B} \end{cases} ; \quad S_B^*(\omega) = (\gamma + \delta u_*)\, e^{-\varepsilon(\omega - \omega_1)} \tag{E.6}$$

$$S_B(k) = \begin{cases} S_A(k) \\ \text{Max}\left[S_A(k), S_B^*(k)\right] \end{cases} ; \quad S_B^*(k) = \frac{1}{2}(\gamma + \delta u_*)\left(\frac{g}{k}\right)^{1/2} e^{-\varepsilon g^{1/2}\left(k^{1/2} - k_1^{1/2}\right)} \tag{E.7}$$

Parameters:

$\omega_1 = 4\pi/10$
$\omega_B = 6\pi(u_{*m}/u_*)$
$k_1 = \omega_1^2/g$
$k_B = [(6\pi)^2/g](u_{*m}/u_*)^2$

γ = 0.0543 MKS
δ = 0.002717 MKS
ϵ = 2.53 MKS
u_{*B} = 35.8 cm/s
u_{*m} = 12.0 cm/s
u_* = friction velocity (cm/s)
u_{*m} = minimum friction velocity (cm/s)

C. Kitaigorodskii Range

Frequency: $[\omega_B, \omega_c]$
Wave Number: $[k_B, k_c]$
Dispersion Relationship: $\omega^2 = kg$ (gravity)
Empirical Formulae:

$$S_c(\omega) = \begin{cases} S_c^*(\omega) & \text{for } u_* \le u_{*c} \\ \text{Max}\left[S_B^*(\omega), S_c^*(\omega)\right] & \text{for } u_* > u_{*c} \end{cases} ; \quad S_c^*(\omega) = \frac{\alpha}{\omega_B}\frac{g^2}{\omega^4} \tag{E.8}$$

$$S_c(k) = \begin{cases} S_c^*(k) & \text{for } u_* \le u_{*c} \\ \text{Max}\left[S_B^*(k), S_c^*(k)\right] & \text{for } u_* > u_{*c} \end{cases} ; \quad S_c^*(k) = \frac{\alpha}{2k_B^{1/2}}\frac{1}{k^{5/2}} \tag{E.9}$$

Parameters:

$\omega_c = 6\pi$
$k_c = (6\pi)^2/g$
u_{*c} = 75.76 cm/s

D. Leykin-Rosenberg Range

Frequency: $[\omega_c, \omega_D]$
Wave Number: $[k_c, k_D]$
Dispersion Relationship: $\omega^2 = gk\left(1 + \frac{k^2}{k_m^2}\right)$ (gravity and capillary)
Empirical Formulae:

$$S_D(\omega) = S_E(\omega_D)\frac{\omega}{\omega_D}\frac{1+3F^2(\omega_D/\omega_m)}{1+3F^2(\omega/\omega_m)}\left[\frac{F(\omega/\omega_m)}{F(\omega_D/\omega_m)}\right]^q \tag{E.10}$$

$$F(\Omega) = \left(\frac{\Omega^2}{2} + \sqrt{\frac{\Omega^4}{4} + \frac{1}{27}}\right)^{1/3} + \left(\frac{\Omega^2}{2} - \sqrt{\frac{\Omega^4}{4} + \frac{1}{27}}\right)^{1/3}$$

$$q = \left\{\log\left[S_c^*(k_c)/S_E(k_D)\right]\right\}/\left[\log\left(k_c/k_D\right)\right]$$

$$S_D(k) = S_E(k_D)\left(k/k_D\right)^q \tag{E.11}$$

Parameters:

$\omega_p = 10\pi$
$k_p = k_m F(\omega_p/\omega_m)$
$k_m = (g\rho/\tau)^{1/2} = 363.0 \quad 1/m$
$\omega_m = (gk_m)^{1/2}$

E. Mitsuyasu-Honda Range

Frequency: $[\omega_p, \omega_E]$
Wave Number: $[k_p, k_E]$
Dispersion Relationship: $\omega^2 = gk\left(1 + \frac{k^2}{k_m^2}\right)$ (gravity and capillary)
Empirical Formulae:

$$S_E(\omega) = (\eta/2\pi)(2\pi/\omega)^p \tag{E.12}$$

$$S_E(k) = (\eta/2)\frac{g(2\pi)^{p-1}(1+3k^2/k_m^2)}{[gk(1+k^2/k_m^2)]^{(p+1)/2}} \tag{E.13}$$

Parameters:

$\omega_E = [4\pi\mathcal{E}g^2u_*^3\omega_m^{4/3}/3\eta(2\pi)^p]^{3/(19-3p)}$
$k_E = (\omega_E^2 k_m^2/g)^{1/3}$
$\eta = 0.0000875$ MKS
$p = 5 - \log u_*$
$\mathcal{E} = 1.473\ (10)^{-4}$

F. Cox Range

Frequency: $[\omega_E, \infty]$
Wave Number: $[k_E, \infty]$
Dispersion Relationship: $\omega^2 = gk^3/k_m^2$ (capillary)
Empirical Formulae:

$$S_F(\omega) = \frac{2}{3}\mathcal{E}u_*^3 g^2 \omega_m^{4/3}\omega^{-19/3} \tag{E.14}$$

$$S_F(k) = \mathcal{E}u_*^3 k_m^6 k^{-9} \tag{E.15}$$

It should be noticed that in this model the only environmental factor affecting the resulting spectrum is the friction velocity u*(in cm/s), which is directly related to the wind speed u (in m/s) measured at a certain height h (in m) above the sea surface. In this particular case, the Pierson model was developed with the use of the well-established Cardone curve [K15], experimentally relating u* to u at a specified height h = 19.5 m. This curve is

reproduced here in Fig. E1. The following set of values of u and u* extracted from the Cardone curve will be used in subsequent computations:

u (m/s)	u* (cm/s)
3.5	12.0
7.4	24.0
12.3	48.0
20.6	96.0

In support of the modeling effort on ocean surface scattering, a computer code was developed at NRL to implement the above Pierson model describing the one-dimensional fully-developed spectrum of surface waves in both formats: spectral density (m^2/Hz) versus frequency (Hz) and spectral density (m^3) versus wave number (1/m). Figures E2 and E3 illustrate the typical results for the chosen values of wind speed. Also indicated in Fig. E2 are the six frequency ranges considered by Pierson in developing this model.

So far only wind speed has been taken into consideration in discussing about the surface wave spectrum. In fact, other than the spectral distribution of surface waves, one would also like to learn about how the energy is distributed in various azimuthal directions given the knowledge of the mean wind direction. This turns out to be essential information if one desires to obtain a more complete picture of scattering from the ocean surface. In general, the scattering strength is influenced by the specific wind direction as strongly implied by all scattering theories. The primary environmental input is always the two-dimensional spectrum of surface waves, not the one-dimensional one.

In reality, much less is known about the two-dimensional or directional spectrum than the one-dimensional spectrum. Present knowledge is based on a very few attempts to measure the directional spectrum, resulting in several empirically-derived descriptions put forward to summarize these observations. Two of the more comprehensive sets of such measurements were performed by Tyler et al [K8], who employed the radio wave synthetic aperture technique, and Mitsuyasu et al [K6], who made their measurements using the cloverleaf buoy. In this effort, we will use the azimuthal distribution model proposed by Mitsuyasu et al in combination with the Pierson one-dimensional model to construct a two-dimensional spectrum of surface waves.

The two-dimensional spectrum $S_2(f,\theta)$ can be expressed in the form

$$S_2(f,\theta) = S_1(f)\,A(f,\theta) \quad , \tag{E.16}$$

where $S_1(f)$ is the one-dimensional spectrum and $A(f,\theta)$ is an angular distribution function with θ denoting the angle relative with the wind direction. The function $A(f,\theta)$ should be normalized such that

$$\int_0^{2\pi} A(f,\theta)\, d\theta = 1 . \tag{E.17}$$

In deriving a specific form for A(f,θ), Mitsuyasu et al assumed the following analytical form for A(f,θ)

$$A(f,\theta) = N(s)\left|\cos\frac{\theta}{2}\right|^{2s} \tag{E.18}$$

of which the parameter s was a function of frequency determined by fitting the observed data to this assumed form and the function N(s) was specified via the normalization condition of Eq. (E.17), leading to

$$N(s) = \frac{1}{\pi}\, 2^{2s-1}\, \frac{\Gamma^2(s+1)}{\Gamma(2s+1)} \tag{E.19}$$

where Γ is the Gamma function.

The function A(f,θ), as prescribed by Eq. (E.18), represents a symmetric bell-shaped distribution centered about the wind direction, the width of which depends solely on the frequency-dependent value of the fitting parameter s(f). Figure E4 ilustrates this angular distribution for representative values of s. There it is seen that most of the energy is strongly concentrated in the wind direction for high values of s while it is more evenly spread out if the values of s are low. The exact functional dependence of s proposed in the Mitsuyasu model was given as

$$s = \begin{cases} s_o \tilde{f}^{-2.5}, & \tilde{f} \geq \tilde{f}_m \\ s_o \tilde{f}^{5}/\tilde{f}_m^{7.5}, & \tilde{f} < \tilde{f}_m \end{cases} \tag{E.20}$$

where $\tilde{f}$ is the dimensionless frequency defined by $\tilde{f} = \omega u/g$, $\tilde{f}_m$ denotes this quantity corresponding to the peak frequency of S_1, and $s_o = 11.5$, a fitting constant. The above estimate of the s parameter is a reasonable representation of the presented data except at the maximum $\tilde{f} = \tilde{f}_m$, where s undergoes a rather sudden change in value in the form of a very sharp peak. Here we propose to remove this unrealistic behavior of s(f) at $\tilde{f} = \tilde{f}_m$ by replacing the fitting expression of Eq. (E.20) with a slightly different expression for s(f) without significantly changing the original estimate for s(f). The modified fitting formula is

$$s = \begin{cases} s_o \tilde{f}^{-2.5} \exp\left[-(\tilde{f}_m/\tilde{f})^{5/2}\right], & \tilde{f} \geq \tilde{f}_m \\ s_o (\tilde{f}^5/\tilde{f}_m^{7.5}) \exp\left[-(\tilde{f}/\tilde{f}_m)^5\right], & \tilde{f} < \tilde{f}_m \end{cases} . \tag{E.21}$$

Both estimates of s(f), original and modified, are presented in Fig. E5 for the four chosen values of wind speed. This demonstrates that the modified expression for s(f) is not substantially different from the original one proposed by Mitsuyasu et al, making it realistically well-behaved near the peak

frequency. Figures E4 and E5 combined show that the Mitsuyasu azimuthal dependence predicts that the angular distribution will be relatively well-focused near the peak frequency and become broader as the frequency goes farther away from it.

In applying the Mitsuyasu distribution to construct a two-dimensional spectrum, we substitute $S_1(f)$ with the Pierson one-dimensional fully-developed spectrum. This will result in a complete description of the surface wave intensity in both spectral and angular dimensions. With this representation for the ocean surface waves, we have the necessary information required for input into all surface scattering models of interest. A graphical illustration of the two-dimensional spectrum is presented in Fig. E6 for a typical value of wind speed. Therefore, on the basis of Mitsuyasu's model of azimuthal dependence, variation of the surface wave spectrum as a function of the azimuth is only significant for a limited frequency range about the peak frequency. The implications of this on acoustic surface scattering is that the directionality will be frequency dependent for a developed sea and potentially vary at a fixed frequency as the sea develops. This shows that extremely careful experimental measures will be required to test these combined acoustic and surface wave hypotheses.

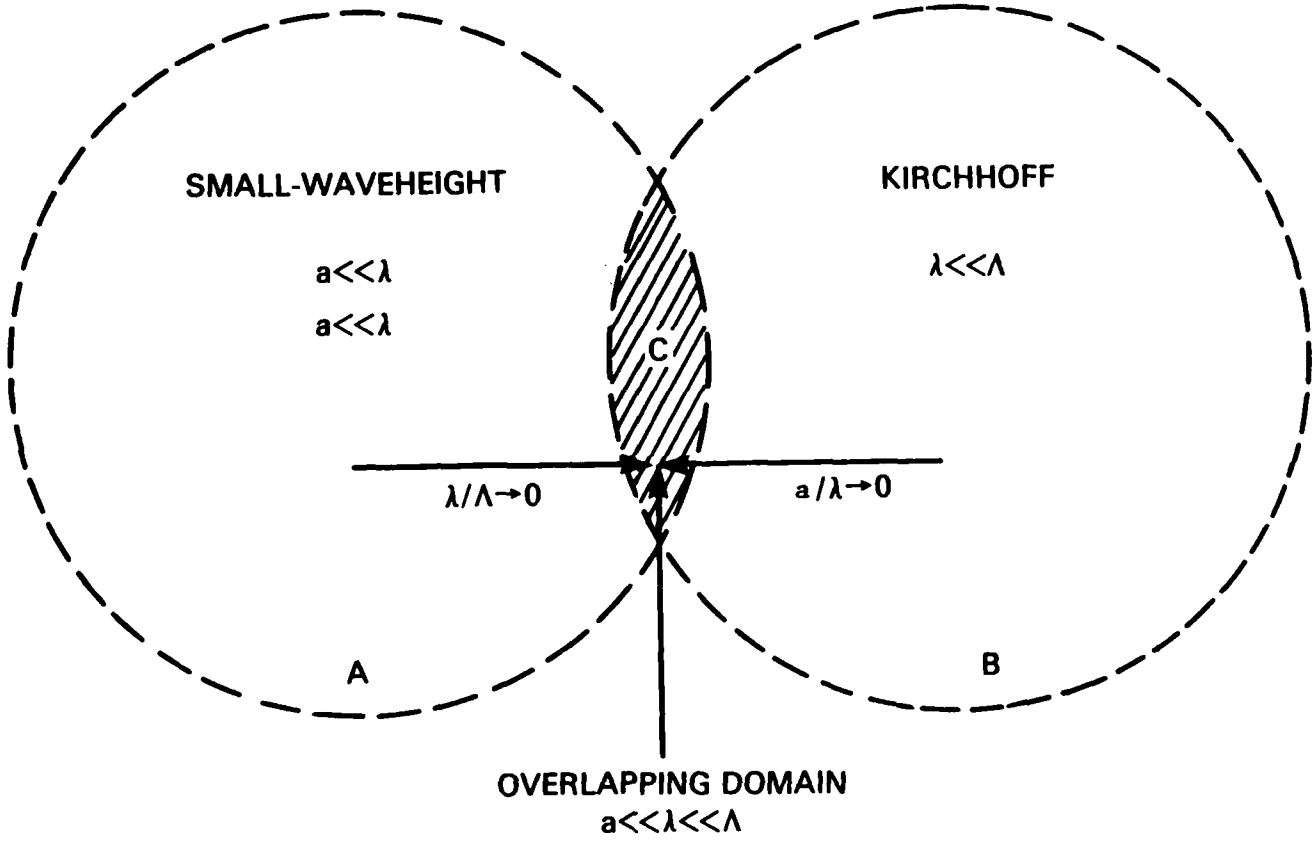

Fig. 1 — Validity domains of the small-waveheight and Kirchhoff approximations with their overlapping region [C1].

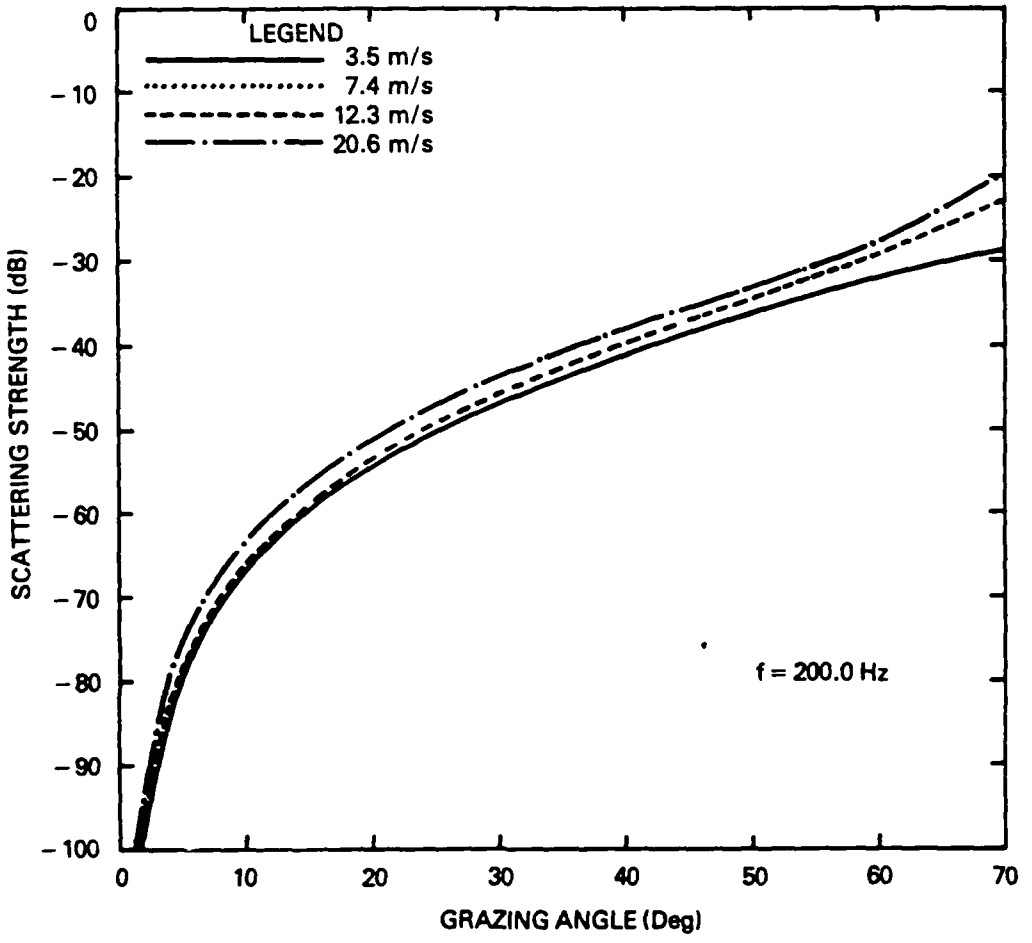

Fig. 2 — Variation of the isotropic backscattering strength with wind speed computed by the first-order perturbation method at acoustic frequencies of a) 200 Hz and b) 50 Hz.

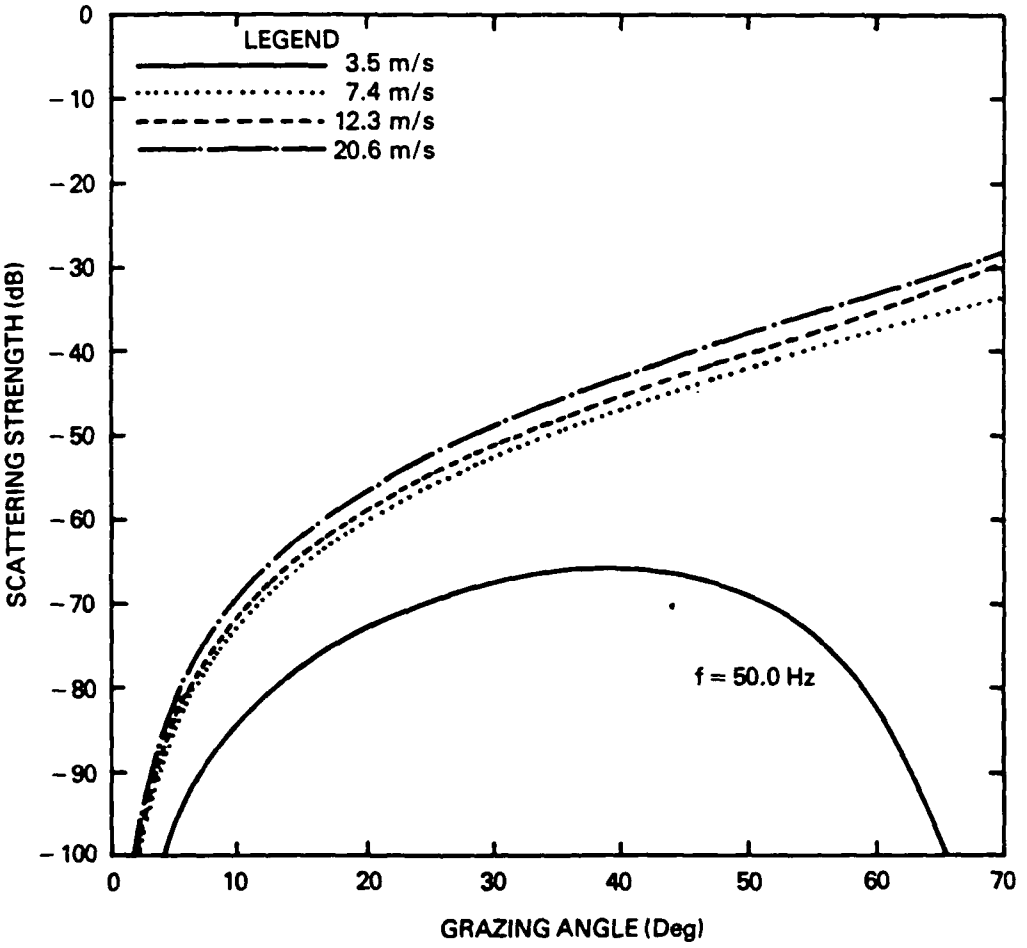

Fig. 2 — (Continued) Variation of the isotropic backscttering strength with wind speed computed by the first-order perturbation method at acoustic frequencies of a) 200 Hz and b) 50 Hz.

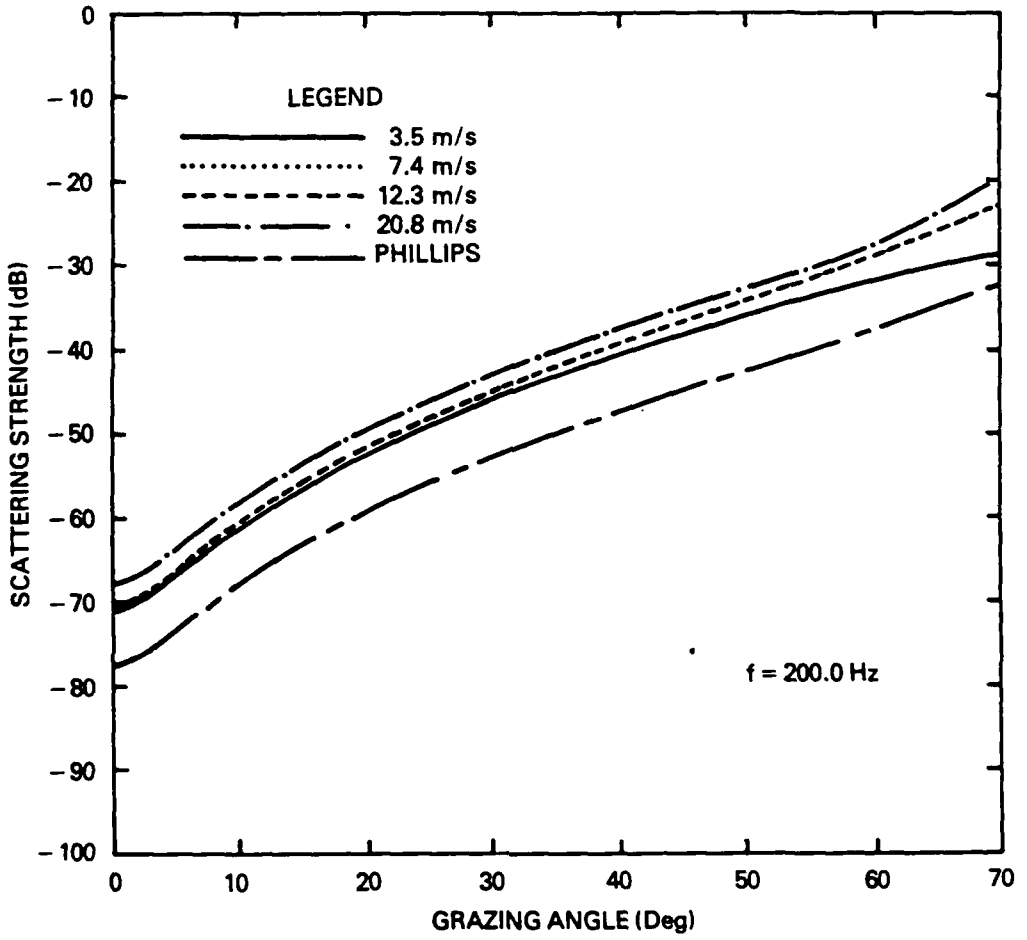

Fig. 3 — Variation of the isotropic backscattering strength with wind speed computed by the composite-roughness approach at acoustic frequency of 200 Hz. Different ocean surface models used as input to this solution are compared between the Phillips spectrum and the six-range Pierson spectrum adapted in the present report.

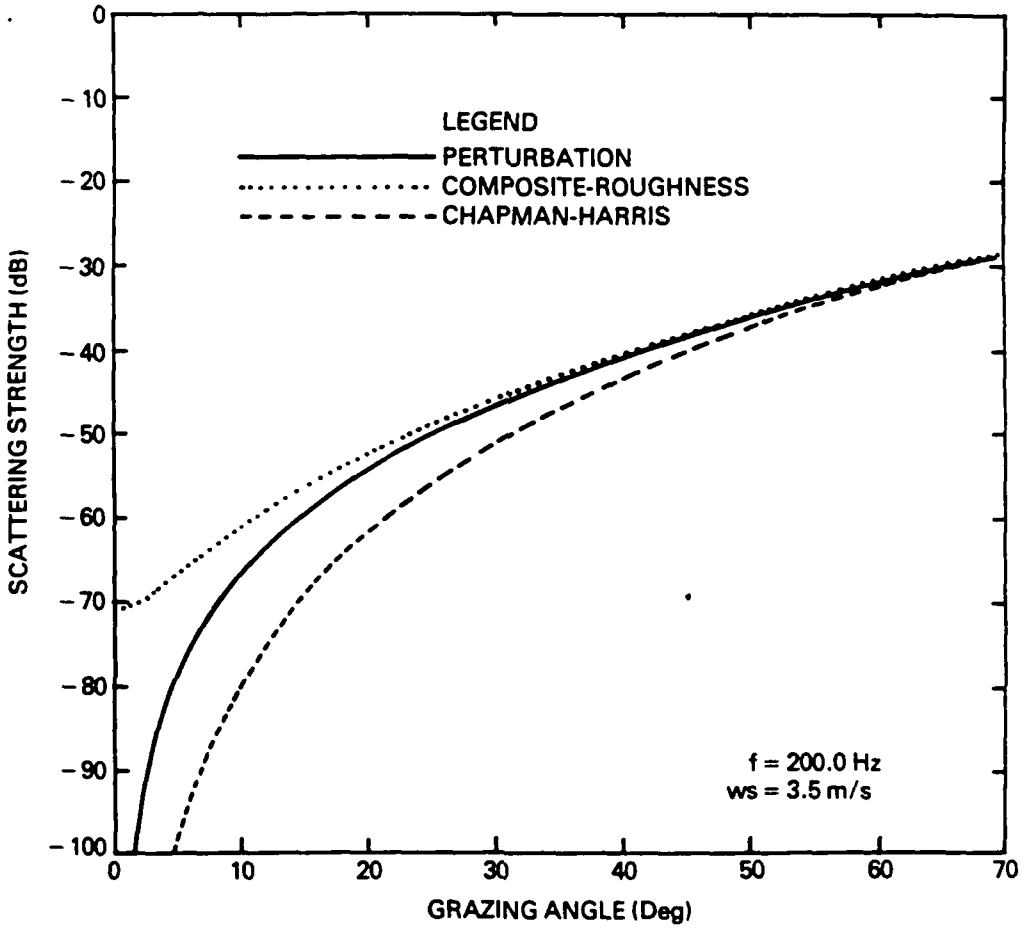

Fig. 4 — Isotropic backscattering strengths computed by three surface scattering models (first-order perturbation, composite-roughness and Chapman-Harris) are compared for acoustic frequency of 200 Hz and wind speed of 3.5 m/s.

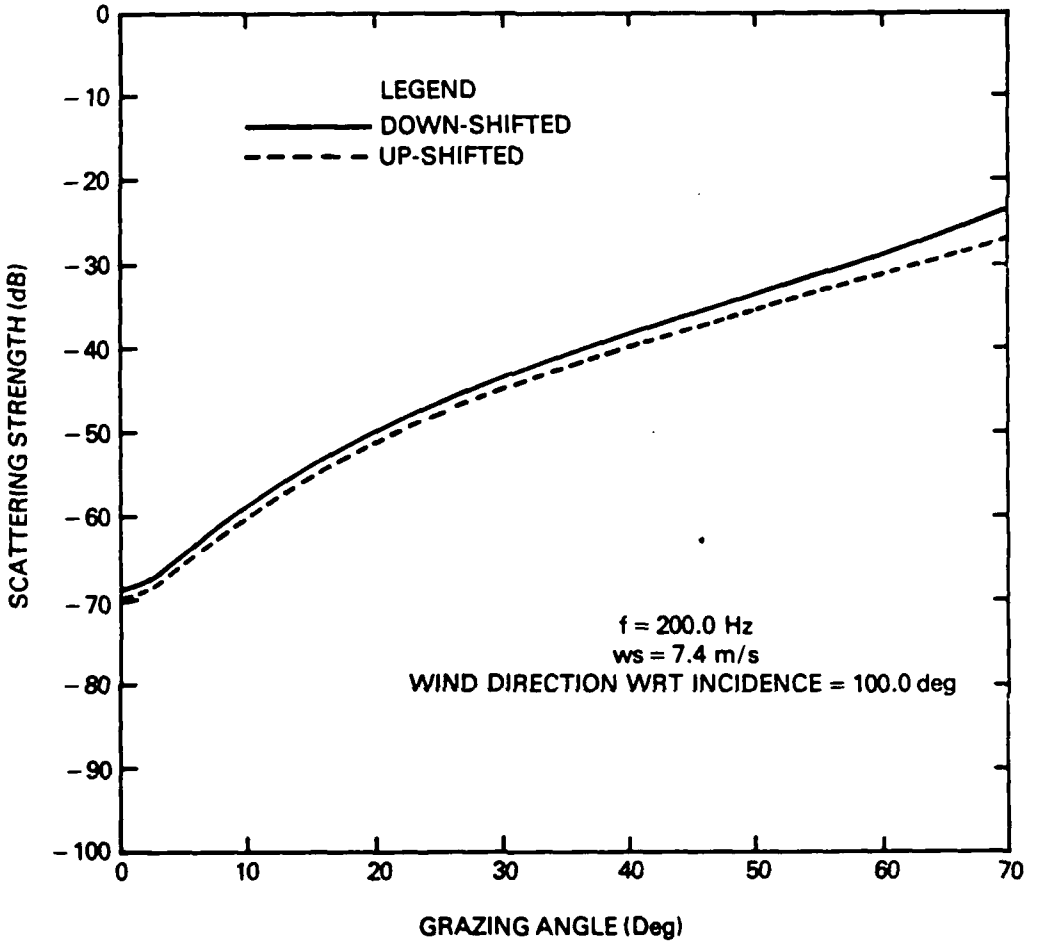

Fig. 5 — The up-shifted and down-shifted components of the backscattering strength computed by the composite-roughness model are evaluated for four different wind directions (with respect to the incident direction projected on the surface): a) 100 deg (almost cross-wind); b) 120 deg; c) 150 deg; d) 180 deg (up-wind).

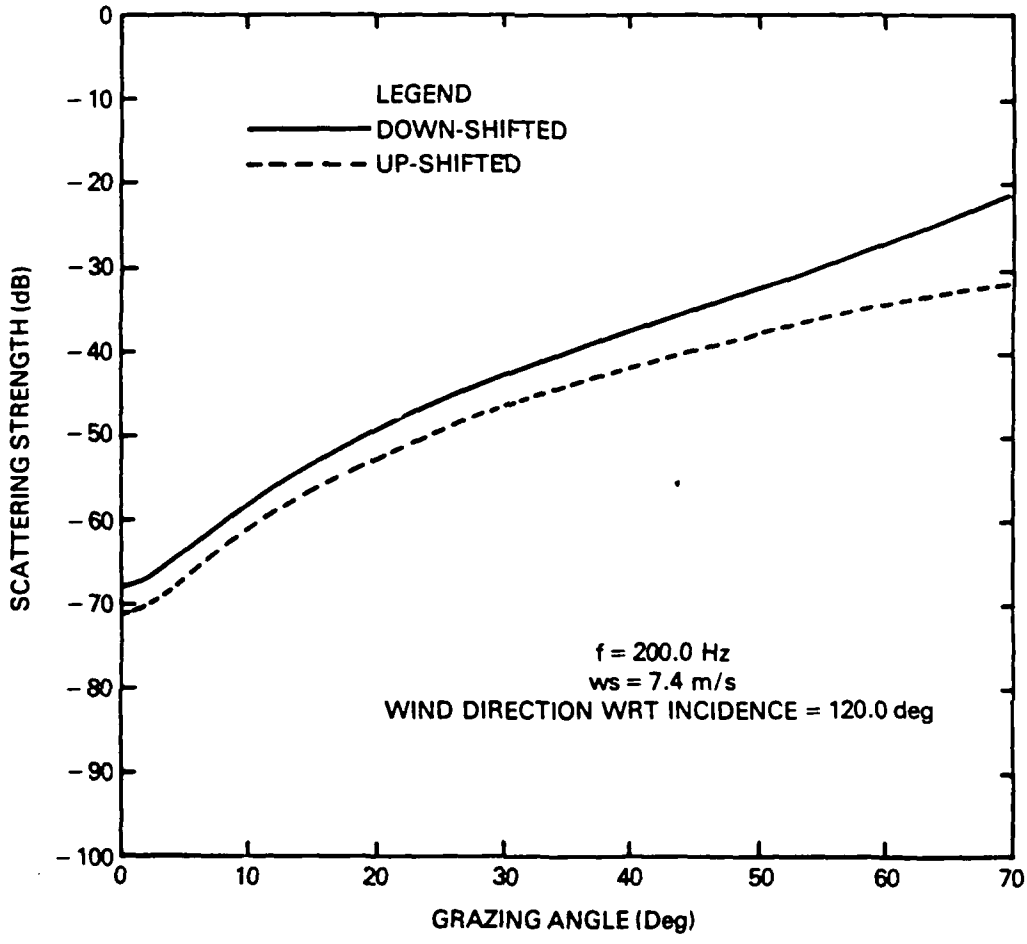

Fig. 5 — (Continued) The up-shifted and down-shifted components of the backscattering strength computed by the composite-roughness model are evaluated for four different wind directions (with respect to the incident direction projected on the surface): a) 100 deg (almost cross-wind); b) 120 deg; c) 150 deg; d) 180 deg (up-wind).

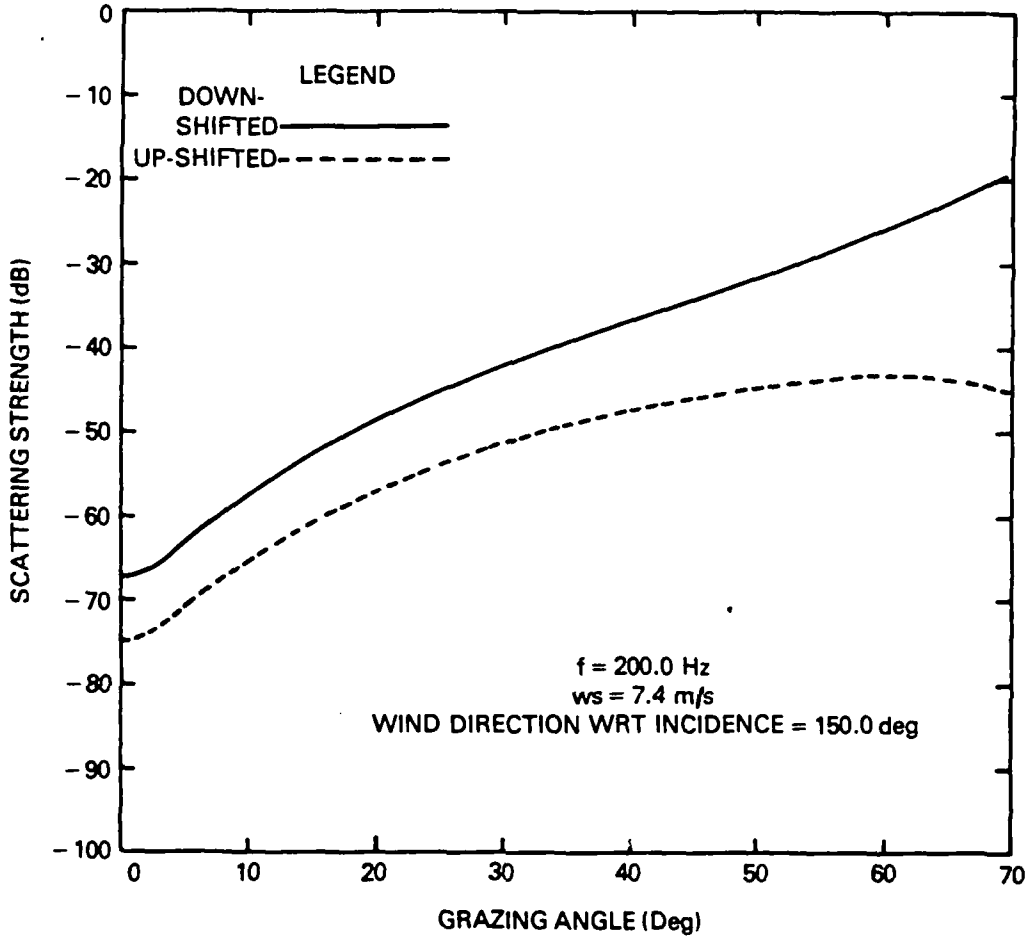

Fig. 5 — (Continued) The up-shifted and down-shifted components of the backscattering strength computed by the composite-roughness model are evaluated for four different wind directions (with respect to the incident direction projected on the surface): a) 100 deg (almost cross-wind); b) 120 deg; c) 150 deg; d) 180 deg (up-wind).

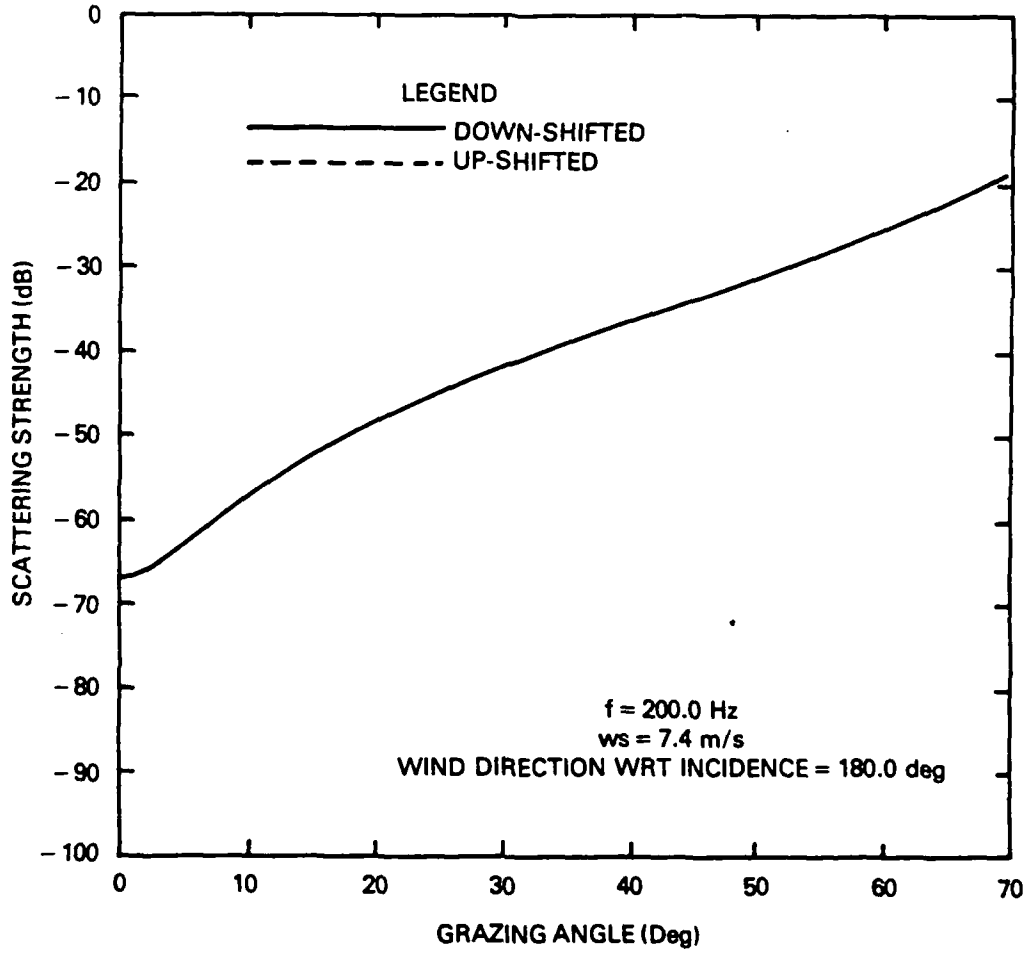

Fig. 5 — (Continued) The up-shifted and down-shifted components of the backscattering strength computed by the composite-roughness model are evaluated for four different wind directions (with respect to the incident direction projected on the surface): a) 100 deg (almost cross-wind); b) 120 deg; c) 150 deg; d) 180 deg (up-wind).

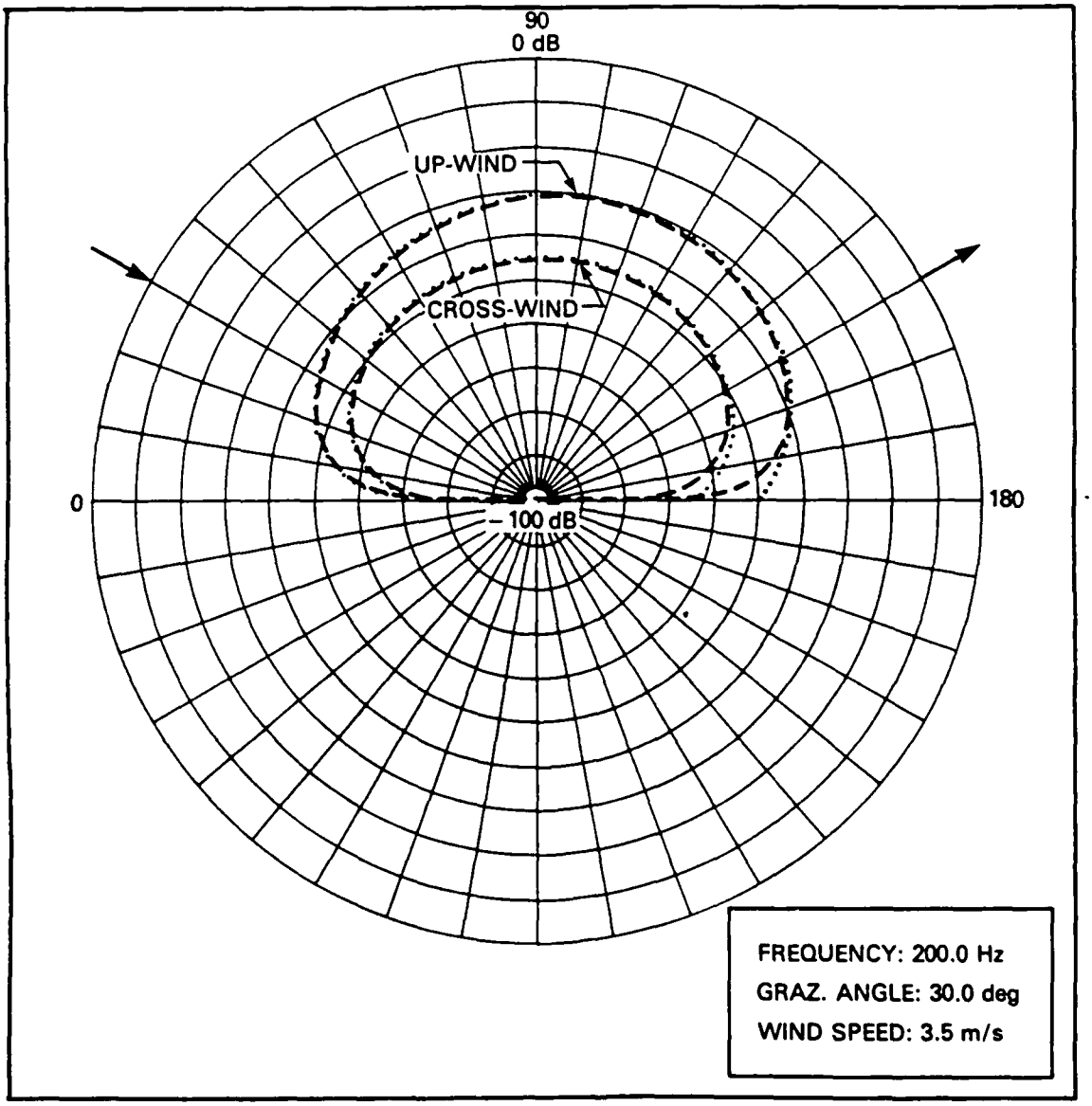

Fig. 6 — The incoherent (up-shifted plus down-shifte) scattering strength as a function of the scattering angle with the incident grazing angle being 30 deg. Computations are performed using both the perturbation and composite-roughness methods for 200 Hz frequency and 3.5 m/s wind speed under two different wind conditions: cross-wind and up-wind.

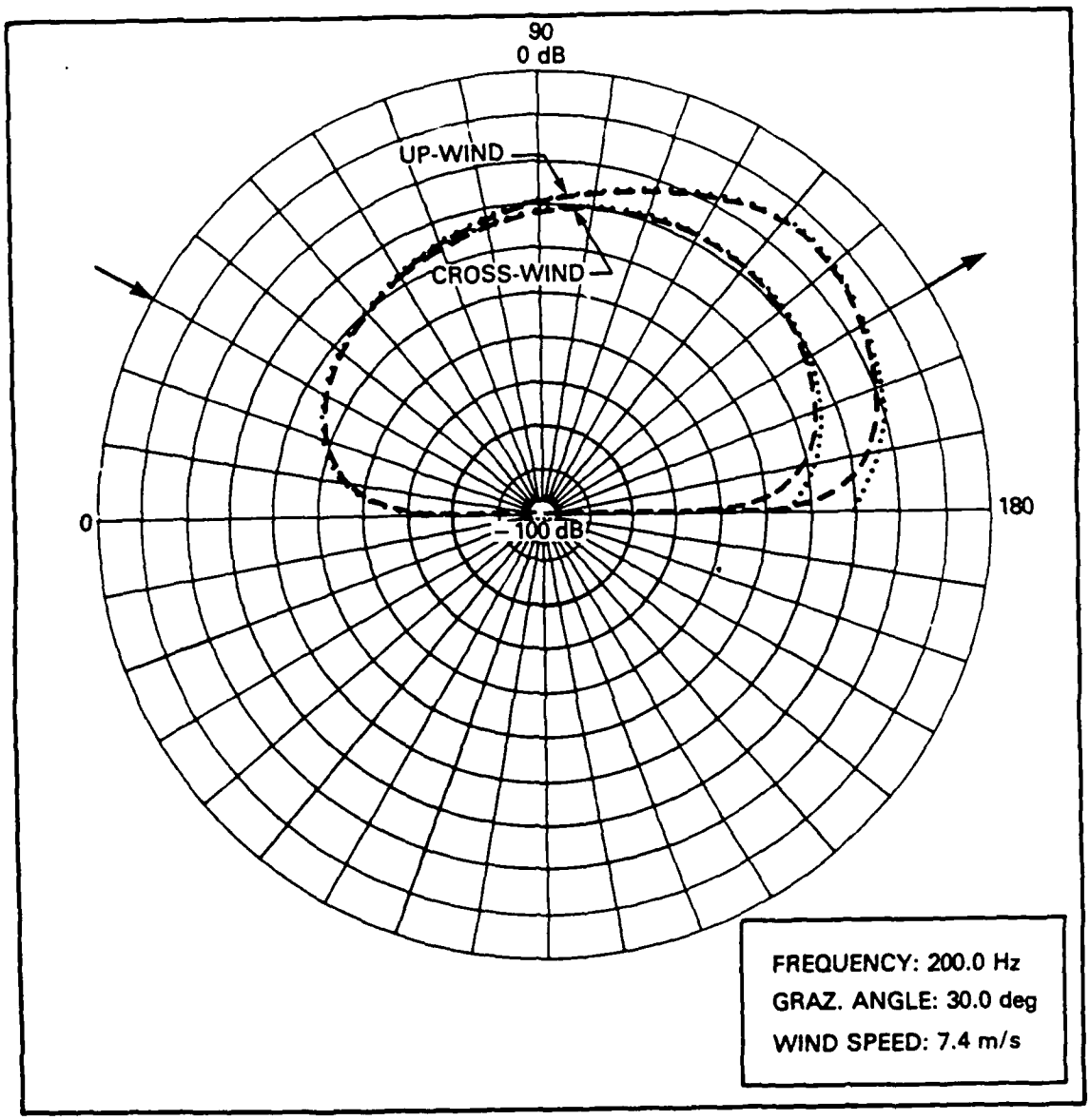

Fig. 7 — Similar computations as in Fig. 6 are performed except for a higher wind speed of 7.4 m/s.

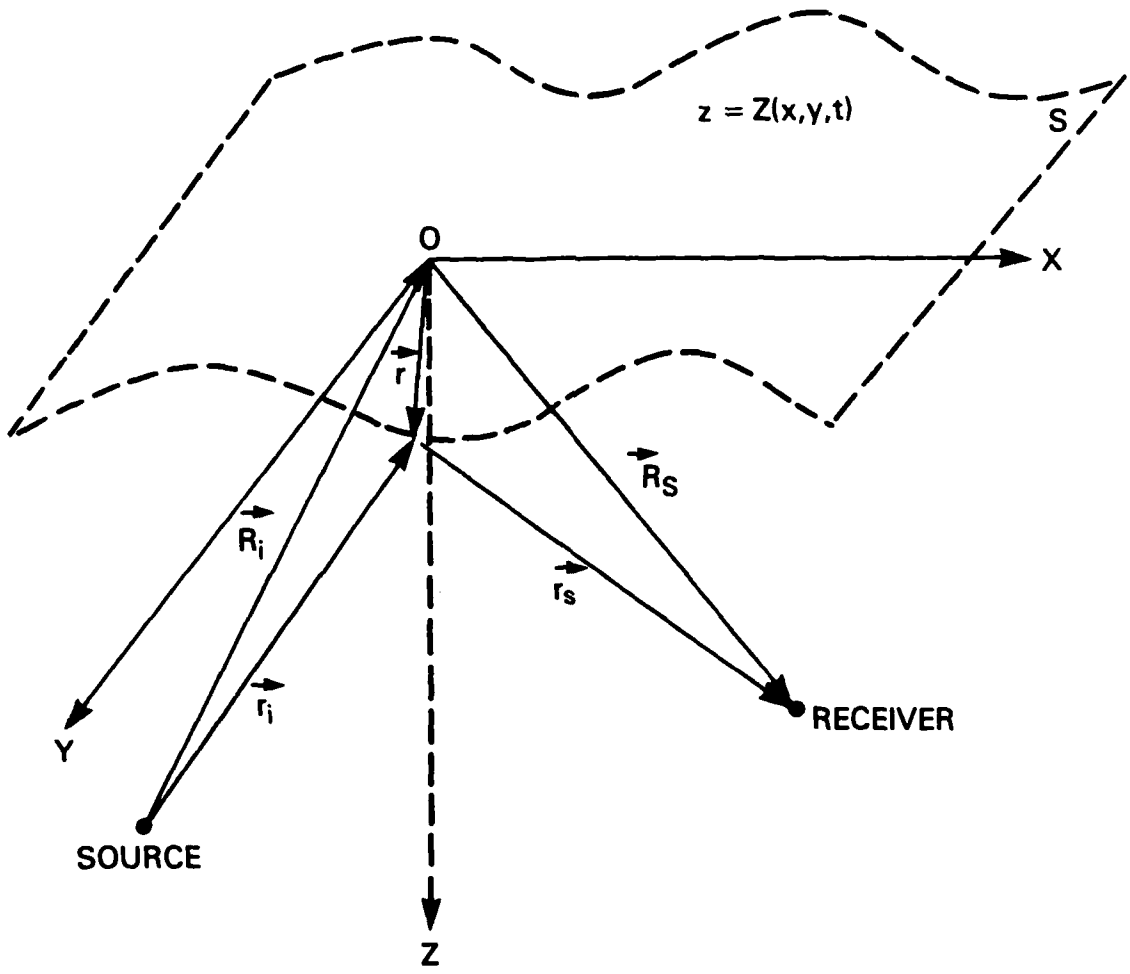

Fig. A1 — Scattering geometry and coordinate system employed in discussions on the tangent plane method.

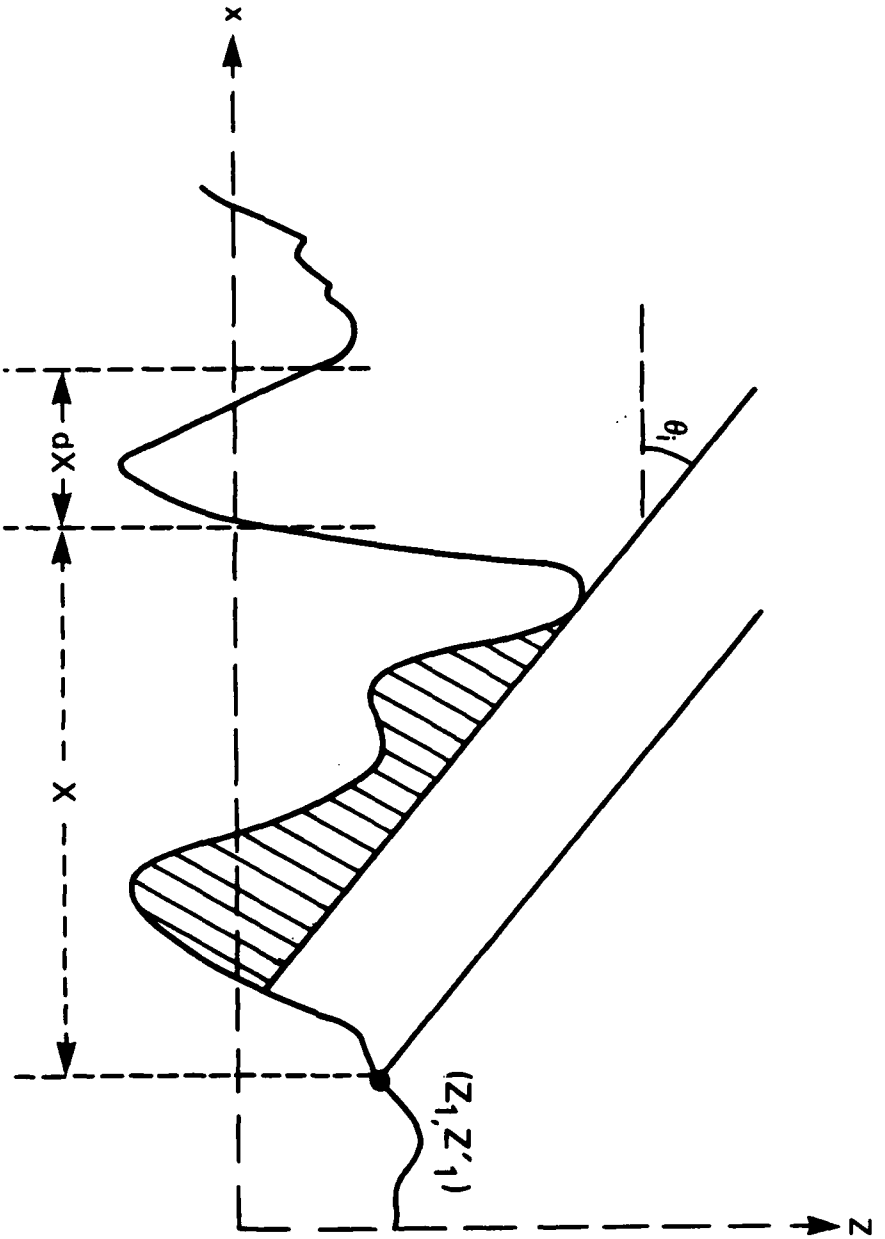

Fig. A2 — Rough surface shadowing geometry

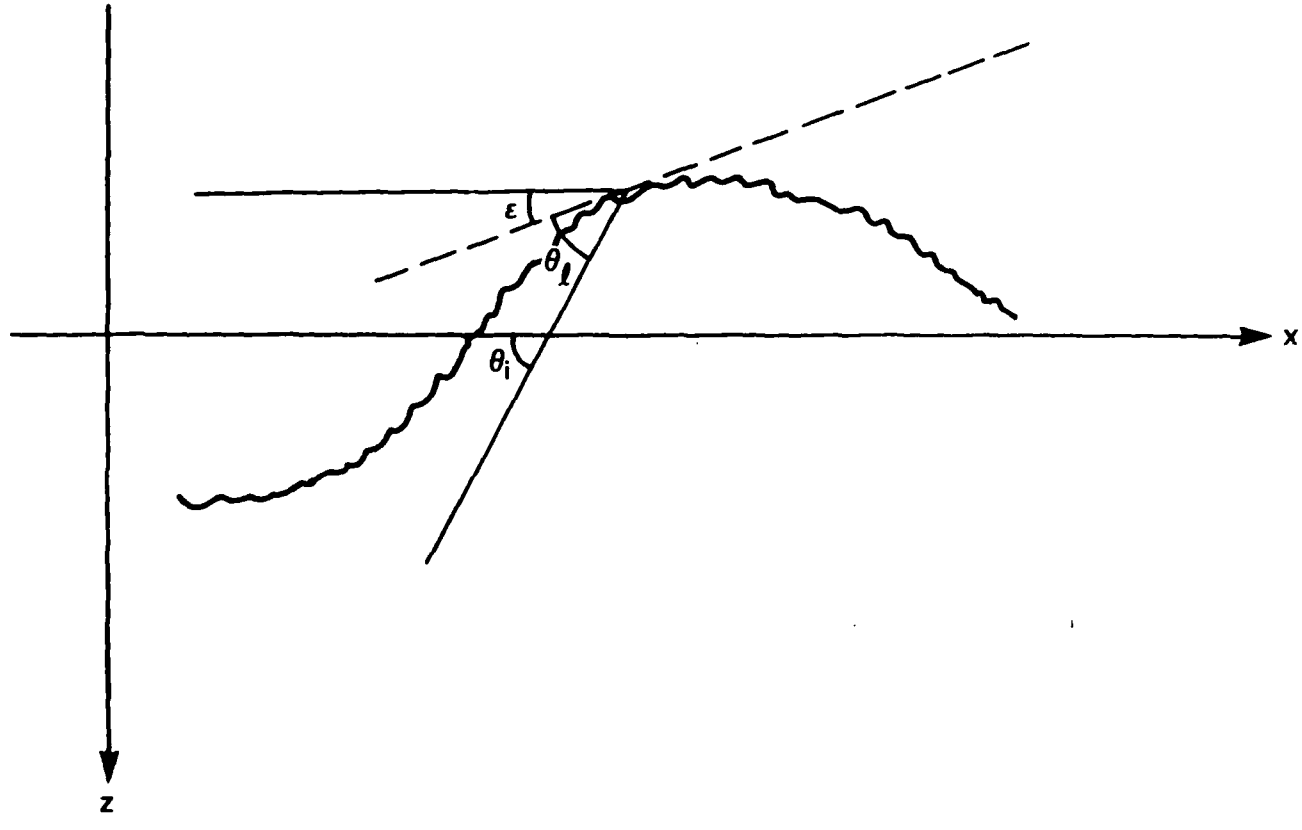

Fig. C1 — Physical picture of the composite-roughness approach

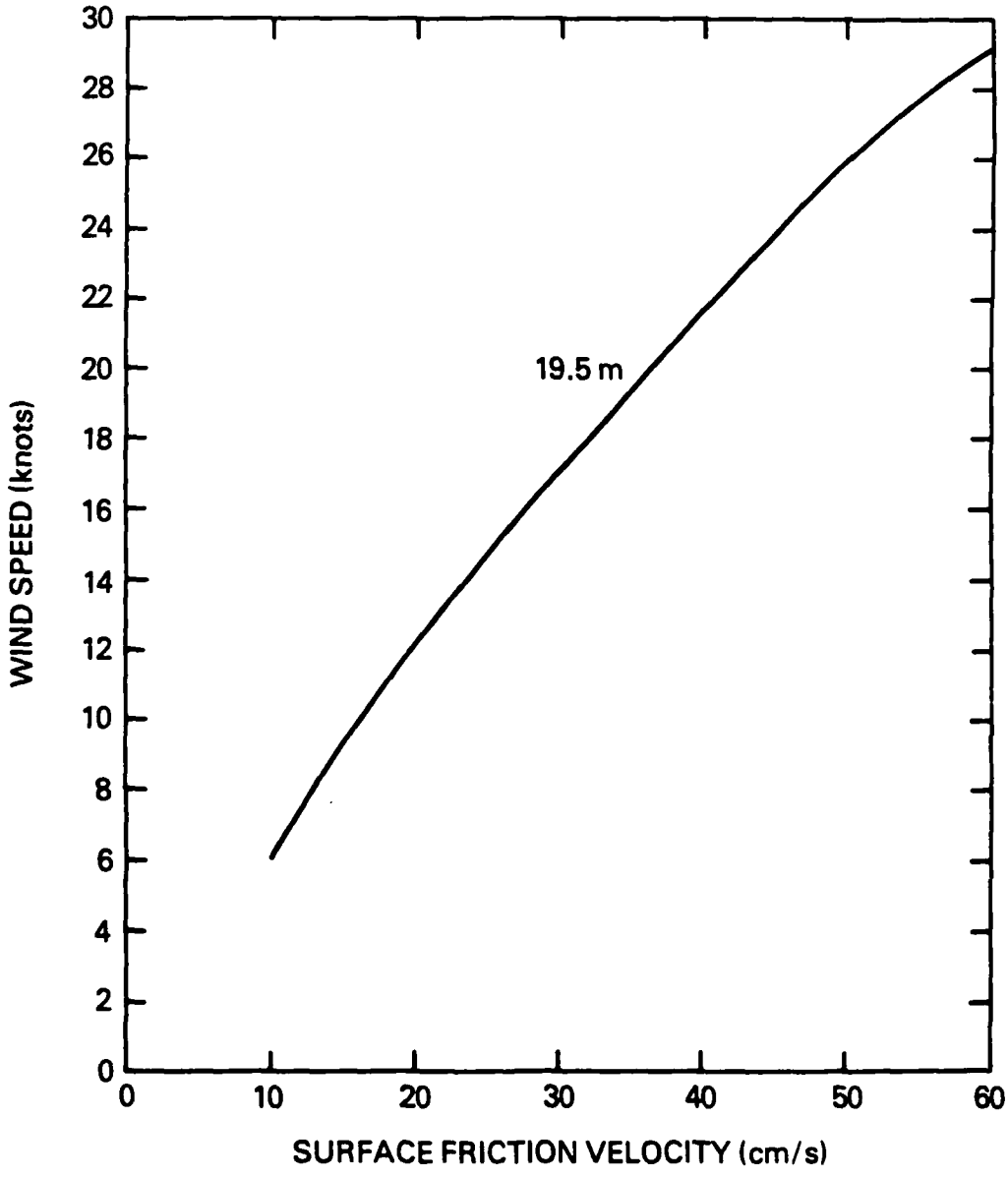

Fig. E1 — The Cardone curve relating the surface friction velocity and wind speed

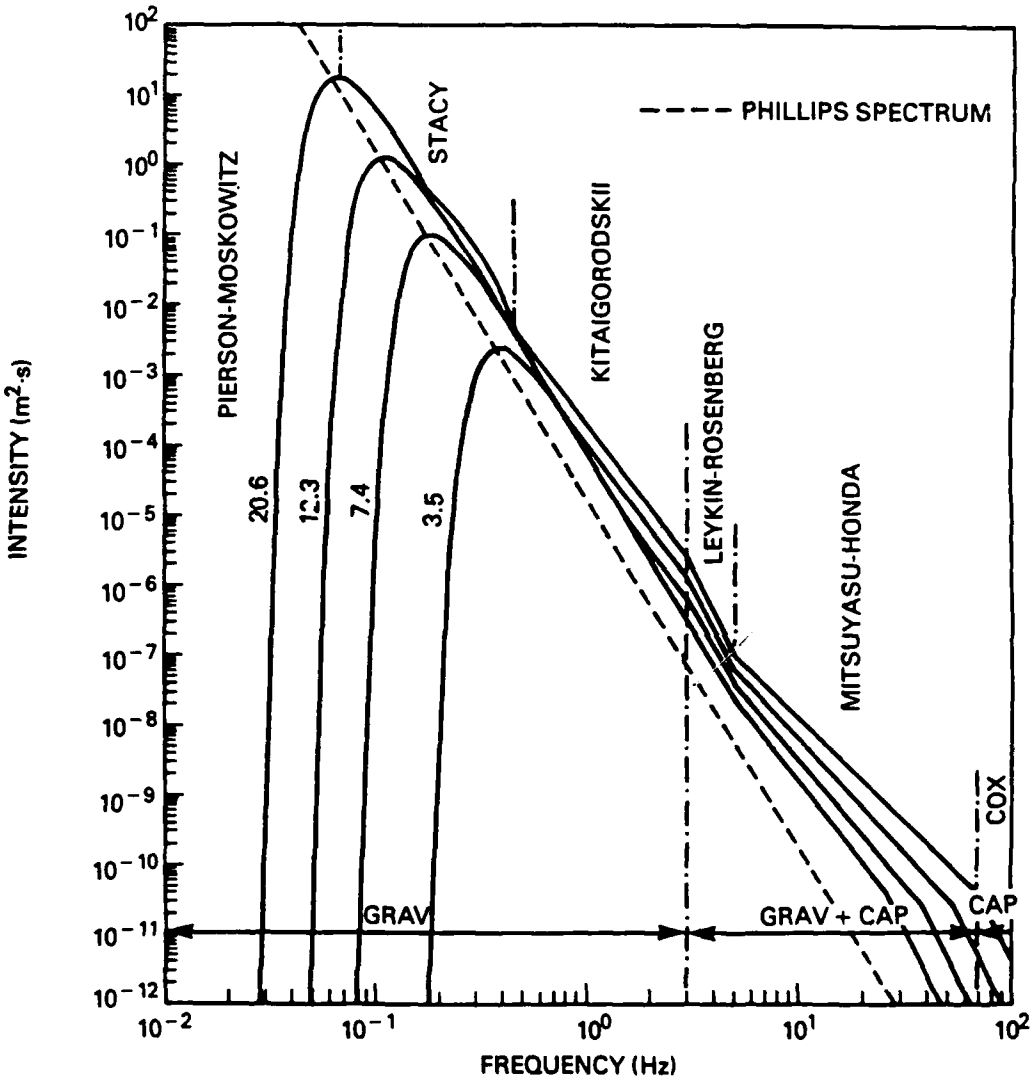

Fig. E2 — Six-range Pierson's model of one-dimensional fully-developed spectrum of ocean surface waves in the frequency domain.

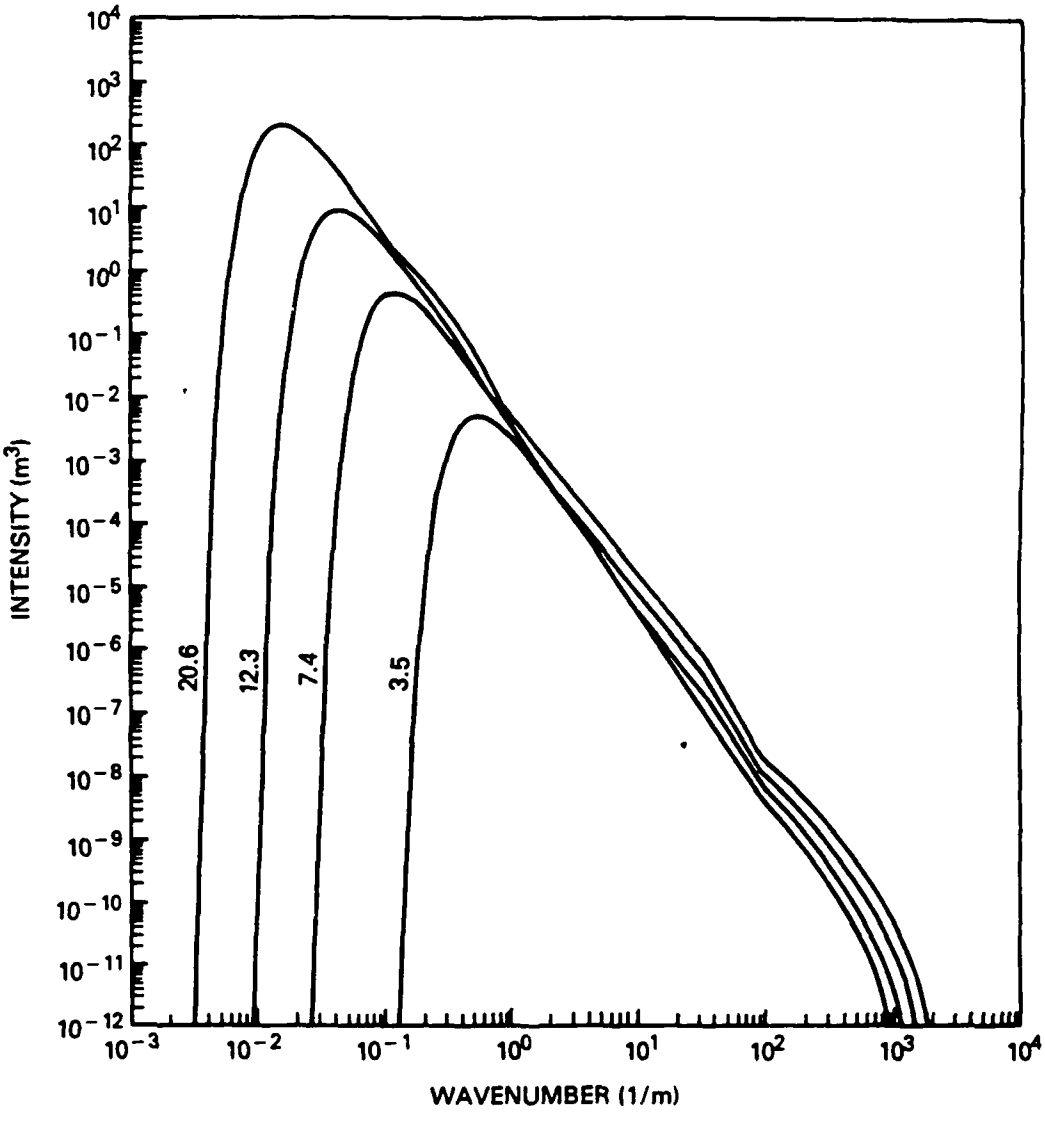

Fig. E3 — The same Pierson's model as in Fig. E2 expressed in the wave number domain

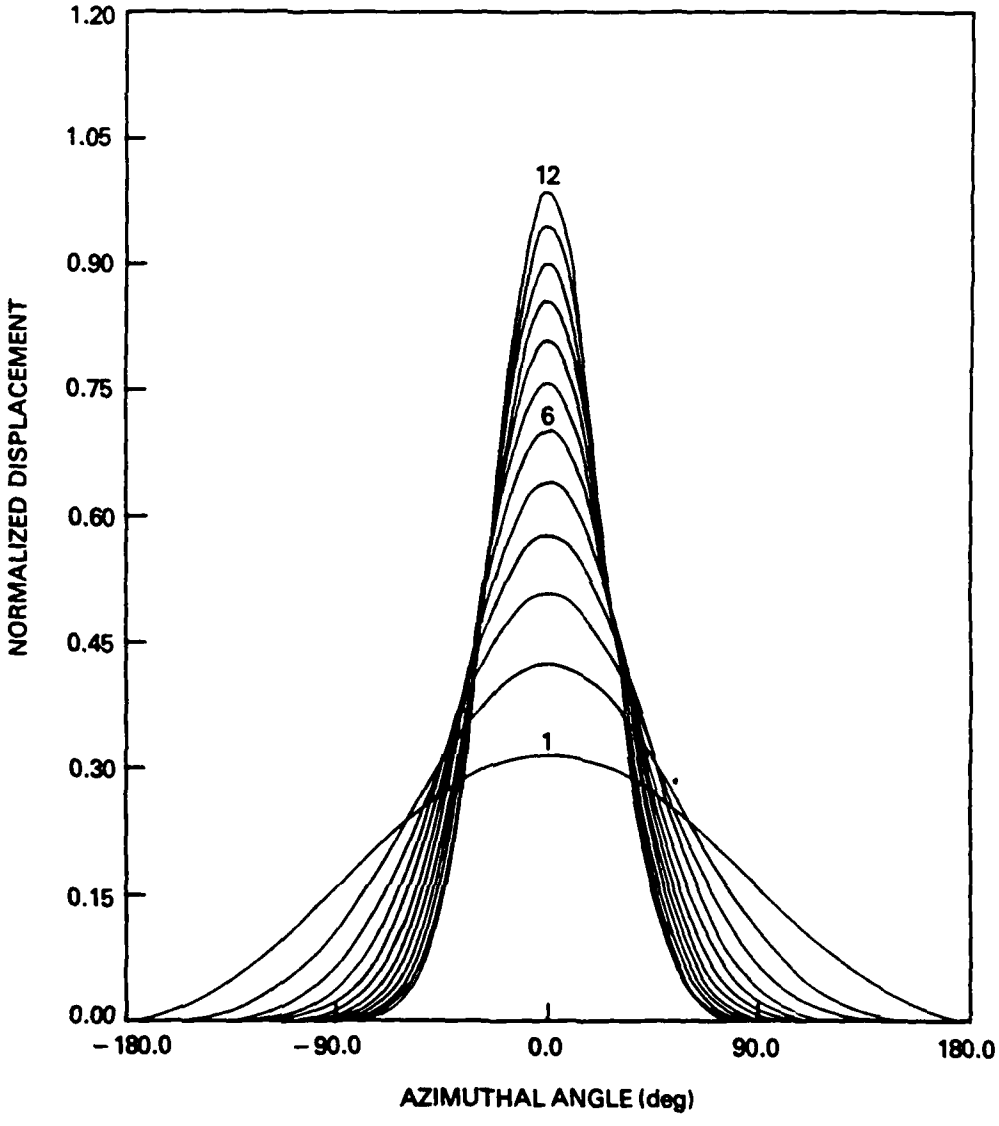

Fig. E4 — The angular distribution function proposed by Mitsuyasu et al to describe the azimuthal dependence of the two-dimensional surface wave spectrum.

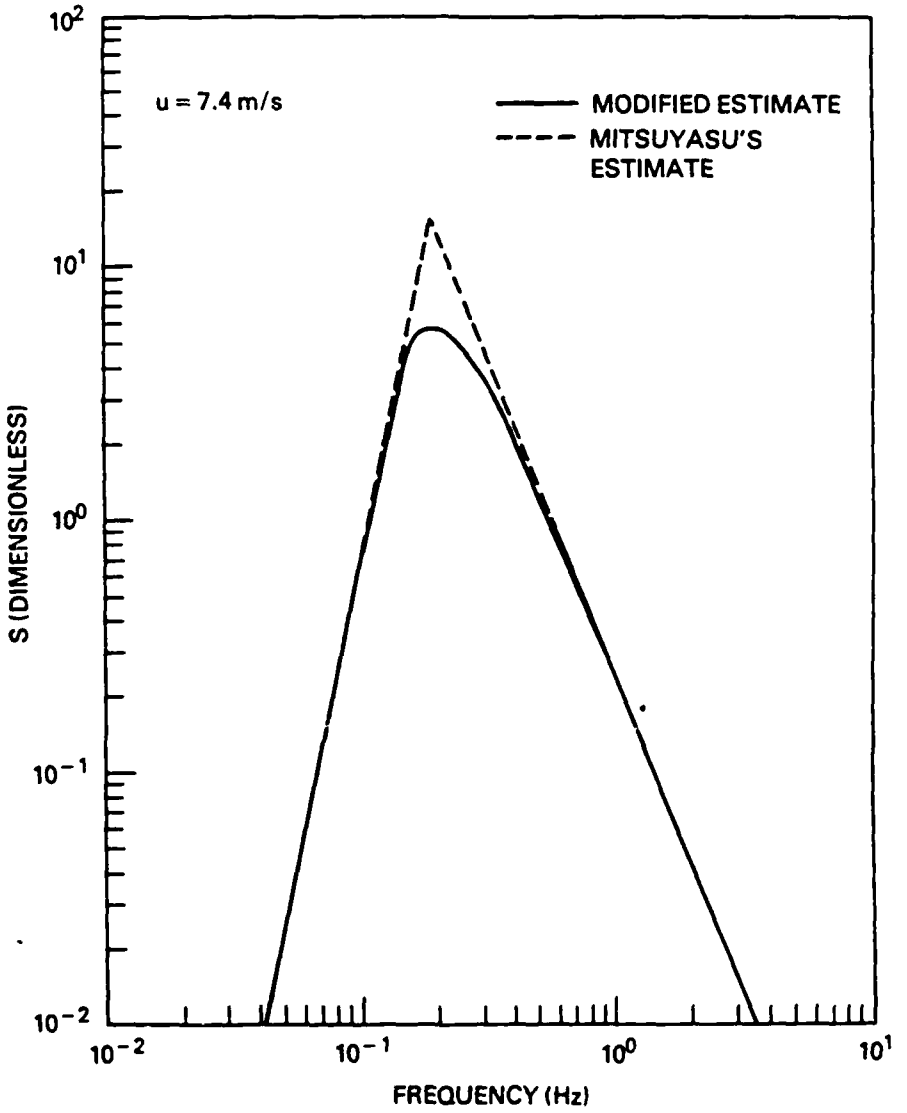

Fig. E5 — Empirical estimates of the s parameters for a given wind speed of 7.4 m/s. Both Mitsuyasu's original estimate and our modification are presented for comparison.

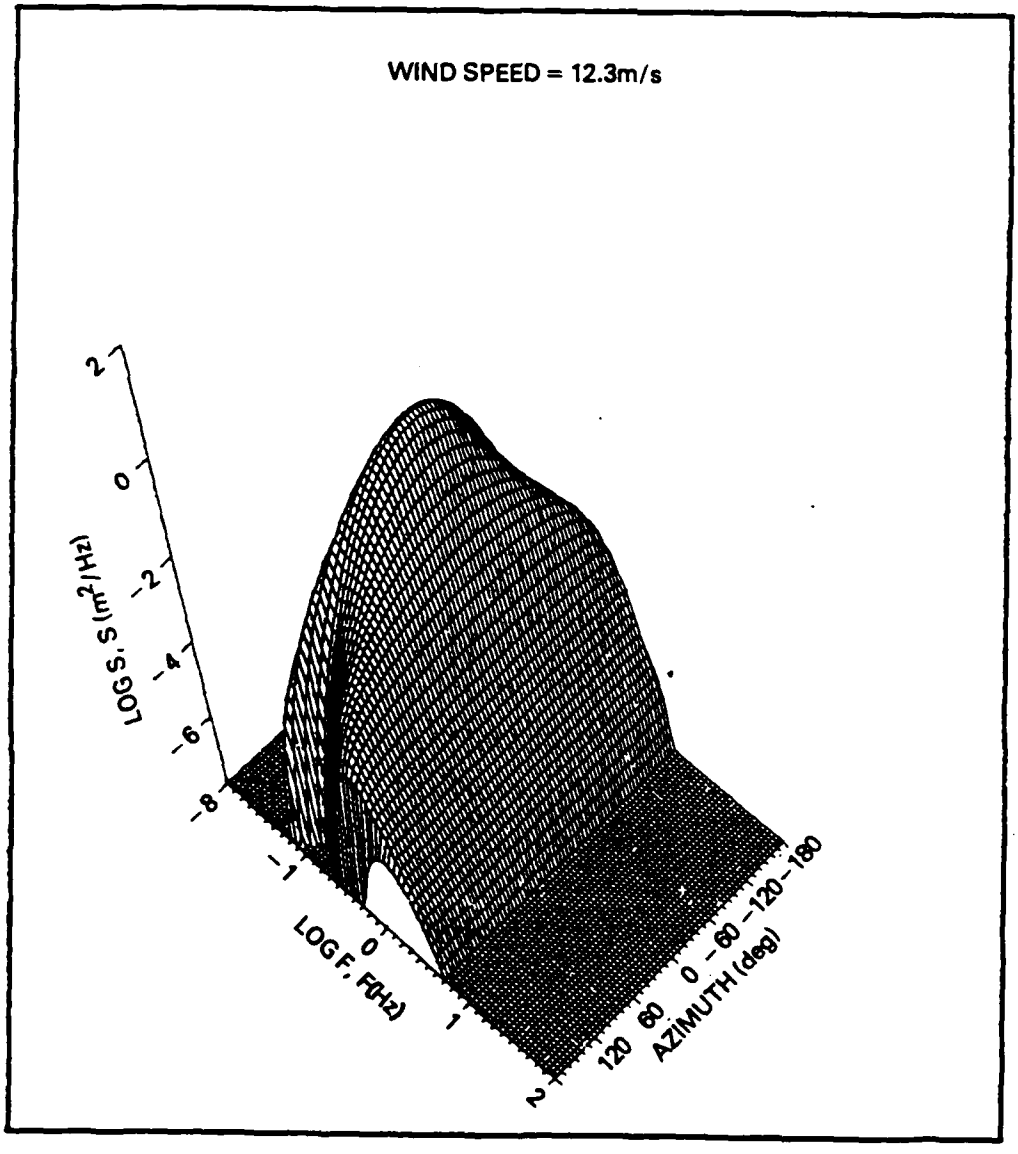

Fig. E6 — Two dimensional spectrum of surface wave constructed from a combinations of Pierson's and Mitsuyasu's models is illustrated for a typical wind speed of 12.3 m/s.